RESPONSE OF A LIGHT AIRPLANE TO RUNWAY ROUGHNESS

BY

D. V. SRIKANTAIAH

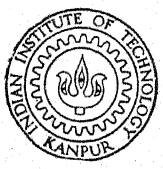

DEPARTMENT OF AERONAUTICAL ENGINEERING

INDIAN INSTITUTE OF TECHNOLOGY KANPUR

AUGUST 1971

RESPONSE OF A LIGHT AIRPLANE TO RUNWAY ROUGHNESS

A Thesis Submitted
In Partial Fulfilment of the Requirements
for the Degree of
MASTER OF TECHNOLOGY

BY
D. V. SRIKANTAIAH

to the

DEPARTMENT OF AERONAUTICAL ENGINEERING
INDIAN INSTITUTE OF TECHNOLOGY KANPUR
AUGUST 1971

CERTIFICATE

Certified that the thesis 'Response of A Light Airplane to Runway Roughness' is the bonafide work done by Mr. D.V. Srikantaiah under my guidance and has not been submitted elsewhere for the award of a degree.

N.C. Nigam

(N.C. Nigam)
Assistant Professor
Department of Aeronautical Engineering
Indian Institute of Technology, Kanpur

ACKNOWLEDGEMENTS

I wish to express my deep sense of gratitude to Dr. N.C. Nigam for his invaluable guidance and encouragement throughout the course of this work. I wish to thank Mr. P.R. Choudhary, Mr. V.C. Srivastava and others of the Flight Laboratory at I.I.T., Kanpur for their kind help and patience during the experiment. I wish to express my sincere thanks to my friends who helped at various stages in bringing up this thesis. I thank Mr. S. Kumar for the excellent typing of this manuscript.

Lastly, I am ever indebted to my parents and kith and kin for their affection and constant encouragement.

D.V. SRIKANTAIAH

ABSTRACT

Response of a light aircraft with a truss type of undercarriage during taxiing and take-off is calculated. For taxiing, the excitation is assumed to be stationary and the aircraft is idealized to a multidegree lumped parameter model keeping the undercarriage unaltered. During take-off, the excitation is treated as nonstationary and the aircraft is idealized to a single-degree-of-freedom spring-mass system. The response parameters of interest are the root mean square value of the displacement and acceleration at the cockpit and the dynamic stresses in the undercarriage members. The excitation to the system comes from the runway roughness. The measurement and power spectral analysis of runway roughness has also been carried out. The response of the aircraft during taxiing is computed using the power spectral density method and that during take-off is computed by numerical integration of the differential equation of motion. The effect of tyre stiffness on the response is studied. The dynamic stresses in the undercarriage members during taxiing are compared with the static stresses. The results are summarised in tables.

NOMENCLATURE

$A_1, A_2, \ldots$	:	areas of cross-section of undercarriage members
C	:	damping matrix
cov	:	covariance
E	:	Young's modulus
h	:	sampling interval
I	:	moment of inertia and identity matrix
K, K'	:	stiffness matrices
k	:	tyre stiffness
K_e	:	equivalent stiffness of wing
$L_1, L_2 \ldots$	:	lengths of undercarriage members
M	:	mass matrix
m	:	correlation lag value and mass
$m_1, m_2, \ldots$	:	elements of M
P	:	displacement vector in normal coordinates
$p_1, p_2 \ldots$	:	elements of P
r	:	lag value
$R_y(\tau)$	:	autocorrelation function; $\tau = rh$
S	:	stress matrix
T	:	transformation (direction cosine) matrix
$U_1, U_2, \ldots$	:	mode shapes
X	:	relative displacement vector in generalized coordinates

$x_1, x_2, \ldots$	:	elements of X
x	:	distance along runway
$y(x)$	:	runway profile
$\ddot{y}(t)$	:	base acceleration
Z	:	absolute displacement vector in generalized coordinates
$z_1, z_2, \ldots$	:	elements of Z
β	:	crtitical damping factor
δ	:	change in length
Γ	:	modal participation factor
θ	:	normalized modal column matrix in normal coordinates
σ	:	standard deviation
σ_X^2	:	mean square relative displacement
$\sigma_{\ddot{Z}}^2$	:	mean square absolute acceleration
ω	:	circular frequency (rad./sec.)
ω_i	:	i^{th} natural frequency
Ω	:	spatial frequency (rad./ft.)
$\phi_{\ddot{Y}}(\Omega)$	:	power spectral density of base acceleration [$(ft.^2/sec.^4)/(rad./ft.)$]
$\phi_Y(\omega)$	:	power spectral density of runway roughness [$ft.^2/(rad./ft.)$]

CONTENTS

CHAPTER 1

INTRODUCTION

During taxi, take-off and landing an aircraft is subjected to random dynamic loads which depend on the nature of runway profile (or roughness). The ground induced vibration environment in which the aircraft operates on the ground is significant from the point of view of pilot's ability to read instruments, passenger comfort and structural life of landing gear and certain vulnerable locations in the airframe. The interest in the behaviour of the aircraft during taxi, take-off and landing is thus motivated both by the operational and structural considerations. With the introduction of large flexible aircrafts, the ground loading condition has become more critical. NASA, NACA, RAE and AGARD have undertaken several investigations to study the airplane response to runway roughness. Roughness of several runways have been measured and runways have been catagorized as smooth, rough, etc. on relative basis. The airplane response, such as displacement and acceleration at the centre of gravity of the airplane or at the cockpit, to runway roughness during taxiing and take-off has been determined mostly through experimental procedures. Not much work has been done in finding the airplane response to runway roughness through an analytical approach, probably because of the nonlinear characteristics inherent in the

airplane and the randomness of the runway profile. Tung, Penzien and Horenjeff[9] have computed the dynamic response of supersonic transport airplanes to runway roughness during taxiing and take-off through a deterministic approach, in which the response is computed by numerically integrating the equations of motion of free-free airframe. Nonlinearity of spring and damping forces have been taken into account. They have also discussed a statistical method to calculate the response of airplane to random loading (runway roughness). Recently Kirk and Perry[16] have carried out the analysis of taxiing induced vibrations in a subsonic aircraft (Boeing 707) by the power spectral density method. The airplane has been idealized to a three-degree-of-freedom spring-mass-damper system. In their work, the excitation coming from the runway roughness has been assumed to be stationary and identical on both the main landing wheels. The same assumption will be made in the present work also.

In the present work, the roughness of a runway has been measured and then the dynamic response of a small airplane to runway roughness during taxiing and take-off has been determined through an analytical approach. In formulating, the problem has been treated as a random vibration problem. The airplane under study has a truss type of undercarriage and is idealized to a five-degree-of-freedom lumped parameter system. The main

object of this work is to compute the dynamic stresses in the undercarriage members developed during taxiing and the absolute vertical accelerations at the pilot's portion during taxiing and take-off. In computing the response during taxiing, the excitation to the system is assumed to be stationary. The excitation to the system comes from the roughness of the runway. During take-off at a constant acceleration, the airplane is idealized to a single-degree-of-freedom spring-mass system subjected to nonstationary input and the response is computed by numerical integration of the differential equation of motion. The approach to this kind of problem, as will be presented in the present work, is new in the sense that random vibration approach (power spectral density method) is sought, which seems more realistic because most airplanes operate in random vibration environment. Also, random vibration studies serve as a useful tool in the design and analysis of systems.

In idealizing the airplane to a discrete or lumped parameter model, the undercarriage is kept unaltered and the effect of wing flexibility is included through an equivalent sprung mass. A method of finding equivalent masses and lumped parameter model of the airplane under study is described in Chapter 3. Chapter 2 deals with the measurement and power spectral calculations of the runway roughness. Two methods have been used to measure the runway profile: (i) Surveying

and (ii) profilometer designed by Panchal[1]. The limitations of each method are discussed. The runway selected is I.I.T. Kanpur airstrip. The roughness is presented in the form of power spectral density functions. Chapter 4 deals with the dynamic response of an idealised aircraft during taxiing and take-off. The response is computed in terms of standard deviation or mean square value. The conversion of spectral density of runway roughness to the spectral density of base acceleration the airplane is subjected to during taxiing at constant speed is also dealt in this chapter. Conclusions are given in Chapter 5.

CHAPTER 2

MEASUREMENT AND SPECTRAL DENSITY CALCULATION OF RUNWAY ROUGHNESS

2.1. Introduction

During taxi, take-off and landing the aircraft moves over the runway. It has been found that runway roughness has adverse effects on airplane operation and has posed problems to designers. To determine the response of the aircraft during taxi, one must have sufficient information about the roughness of the runways on which airplanes are going to operate. Such an information can be obtained from samples of measured runway profile records. This chapter deals with the measurement and a brief description of spectral analysis of the runway roughness. The roughness is presented in terms of power spectra.

2.2 Measurement of Roughness

Several methods have been adopted for measurement of runway profiles. The conventional and most commonly used method is surveying. A brief description of different methods used for the runway profile measurement with their limitations is given elsewhere[1]. Panchal[1] designed and fabricated an equipment, called 'Profilometer'or 'Profile Follower', for measuring road surface profiles. His method is faster when compared to other

methods and a continuous record of any length can be obtained. This equipment was used to get a continuous record of the profile of airstrip at I.I.T., Kanpur in the present work. For study of comparison, the runway roughness data was also collected by surveying. A brief description of the profile follower and its use and limitations in measurement of runway profiles are outlined in the following paragraphs.

2.2.1 Profile Follower

The profile follower consists of a small mild steel wheel of 8 inch diameter which follows the road or runway surface profile. The wheel rotates freely on ball bearings fixed over an axle the two ends of which are connected to two mild steel guide bars, as shown in Fig. 2.1. The guide bars slide freely through brass bushes mounted on a channel. This channel is used to fix the profilometer to the front bumper of a jeep or a motor vehicle. The profilometer is heavy enough as to make contact with the ground when vehicle is in motion. The wheel is so designed as to follow completely the profile of a minimum wavelength of one foot.

2.2.2. Instrumentation

Main accessories used with the profile follower to obtain a record of runway elevation profile were: (i) an accelerometer pickup with a vibrationmeter to sense the

vibration of the profile follower's axle and (ii) a strip chart recorder to record the signal transmitted by the vibrationmeter. The pickup was mounted on the axle at the place provided for this purpose. The pickup at its position senses only the vertical acceleration of the axle, the acceleration being provided by the runway unevenness. This signal is fed into the vibrationmeter which integrates the signal twice, giving the displacement of the profile follower's axle, which in turn represents the elevation of the runway profile. A schematic diagram of the instrumentation is shown in Fig. 2.2. An alternator unit with a voltage stabilizer was used to provide power supply to the strip chart recorder. The specifications and details of the instruments are given in the appendix of Ref.1.

2.2.3. Runway Profile Measurement

The profile follower was fixed to the front bumper of a station wagon (jeep) so that it rests vertically on the ground. The accessories (vibrationmeter, strip chart recorder, voltage stabilizer and alternator unit) were put inside the rear portion of the jeep. The pickup was mounted on the axle of the profile follower. Electrical connections were made as shown in Fig. 2.2. The jeep was driven in the middle of the airstrip at a constant speed of 22 m.p.h. Since it was thought that the variations in profile across the airstrip were small compared to that along the airstrip, only a single record was taken.

The irregularities of the airstrip in longitudinal direction were of prime importance and hence, as an average, profile of the mid-section of the airstrip was measured. The paper speed of the recorder was set to 25 mm/sec.

The criteria for selecting a towing speed of 22 m.p.h. of the vehicle are based on two factors:

(i) the wavelength of interest and

(ii) the operating frequency (> 2 cps) and amplitude ranges of the electronic equipments.

The variations of runway elevations in wavelengths ranging from 1 foot to 100 feet were of interest in the present investigation, as the runway profile is made up of superimposed waves of different wavelengths, the amplitude generally becoming larger as the wavelengths increase. The wavelength of interest, speed of the vehicle and frequency of vibration are related by

$$f = \frac{v}{\lambda} \qquad (2.1)$$

where f = frequency (cps)

v = towing speed of the vehicle (ft./sec.)

and λ = wavelength (ft.)

The minimum wavelength of interest (1 ft.) was fixed by the diameter of the follower wheel. Longer wavelengths, according to Eq. (2.1), can be achieved by increasing the towing speed of the vehicle or by decreasing the frequency. But, at higher

speeds (more than 25 m.p.h.) it was found that the vehicle vibration would play part in the measurement of runway profile, and also the pickup used did not have a flat response at frequencies less than 2 cps. It worked satisfactorily at higher frequencies, from 2 cps to 20,000 cps. Taking all these factors into consideration, a towing speed of about 22 m.p.h. was chosen, which would correspond to a maximum wavelength of 16 ft.

A sample of the record of runway profile obtained by profilometer measurement is displayed in Fig. 2.3.

2.2.4. Calibration of Record

The record of the runway profile on the recorder chart paper represents the surface elevations to some vertical scale. These elevations are plotted over a certain mean, this mean corresponding to the locus of the centre of the follower wheel at every instant of time. To fix the vertical scale, the pick-up was mounted on a shaker table and was connected to the strip chart recorder through the vibrationmeter in the laboratory. The connections and settings of switches of instruments were consistent with that during profile measurement. The shaker table was given a known displacement at a particular frequency and a record of the displacement of shaker table was got. The ratio of the displacement on the paper to that of the

shaker table was then calculated. This ratio was calculated for different operating frequencies of the shaker from 2 cps to 30 cps. These ratios were found to be constant and an average of them would fix the vertical scale. In the present work, 1 mm elevation or depression on the record represented 1.2 mm that on the runway.

The constant towing speed of the vehicle and the recorder paper speed would determine the horizontal scale. Corresponding to vehicle speed of 22 m.p.h. and paper speed of 25 mm/sec., 1 mm on record equalled 1.3 ft. along the runway on horizontal scale.

2.2.5. Limitations on Profile Follower Measurement

(i) Since the pickup used did not have a flat response below 2 cps, variations in longer wavelengths of runway profile could not be obtained at low towing speed of the vehicle.

(ii) At larger speeds (more than 25 m.p.h.) it was found that vehicle vibration was excessive causing extraneous vibration of the pickup.

(iii) Maximum wavelength achievable was only 16 ft. though wavelengths upto 100 ft. were of interest.

(iv) In spite of all efforts to maintain constant speed of the vehicle at all instants, there

were some fluctuations in the speed and hence lot of concentration from the driver was required.

(v) Clear records of profiles can be obtained at higher paper speed. Unfortunately, higher paper speed could not be got with the recorder used in this work.

2.2.6. Improvement Over Profile Follower Measurement

The assumption of constant towing speed of the vehicle could be corrected if the fluctuations in the vehicle speed were recorded along with the record of the runway profile simultaneously as a result of which actual heights could be deduced. To achieve this , a 'Make and Break' contactor or 'Timer' (Fig.2.4) was designed and was fixed to the follower wheel. There was one contact made by the timer for every revolution of the wheel. In the present work, the electrical signals from the timer and the pickup were simultaneously recorded. The timer signals at higher towing speeds could not be recorded along with the record of the runway profile due to the smaller diameter of the follower wheel and the paper speed limit. Timer signals could be recorded only at vehicle speeds less than 6 m.p.h. With a follower wheel of larger diameter and a sufficiently higher recorder speed it would be possible to record the timer signals and the runway profile simultaneously.

2.2.7. Measurement of Runway Profile by Surveying

To compensate for the limitation (iii) (Section 2.2.5) and to compare the results of the measurement made by profile follower, the I.I.T., Kanpur airstrip roughness data was also collected from survey measurements. Roughness variations in longer wavelengths can be obtained by surveying. For most airplanes the frequency range between 0.5 and 35 c.p.s. is the region of prime concern[10]. At an airplane speed of 50 m.p.h. this frequency range corresponds to wavelengths between about 150 and 2 ft. Since the variations of runway profile in longer wavelengths of the order of 100 ft. were of interest, a reading interval of 2 ft. was selected which corresponds to a minimum wavelength of 4 ft. Variations in runway profile at wavelengths less than 4 ft. could not be measured by surveying as the staff had a least count of 0.01 ft. Roughness measurements along the mid-longitudinal section of the runway were made by means of a surveyor's level, a tape and a staff. Measurements were made for a total length of 1600 ft. of the runway.

2.3. Power Spectral Density Calculation Of Runway Roughness

The runway profile is a random process with distance as the indexing parameter. It provides the basic data for the excitation of the aircraft as it moves on the runway. If the velocity of the aircraft is known, then runway profile gives the basic motion as a function of time. Collection of several runway profiles thus provides the ensemble for random vibration analysis of the aircraft. However, if the runway profile is assumed to be ergodic a single long record can be used.

The random vibration analysis of the aircraft can be performed in two ways:

1. Time Domain Approach
2. Frequency Domain Approach.

Frequency domain approach is relatively convenient for stationary case and is based on the use of power spectral density functions (PSDF). PSDF gives the spectral characteristics of the profile. As the runway profile exhibits random characteristics which are normally uniform, the stationarity of the random process is assumed in the power spectral calculations.

Since the runway roughness is a spatial disturbance the power spectral density function is defined in terms of the frequency argument Ω in radians per foot rather than the

conventional argument ω in radians per second. If y(x) denotes the runway height - x is distance along the runway - then the power spectral density function, $\phi_Y(\Omega)$, in terms of Ω is defined by

$$\phi_Y(\Omega) = \lim_{X \to \infty} \frac{1}{2\pi X} \left| \int_{-X}^{X} y(x)\, e^{-i\Omega x}\, dx \right|^2 \qquad (2.2)$$

where the bars $|...|$ indicate the modulus of complex quantity. Eq.(2.2) may be used to evaluate the power spectral density function from observed data, but, in practice, the power spectral density may be determined more conveniently and less tediously by making use of a related function, the 'auto-correlation function', $R_Y(\tau)$, defined by

$$R_Y(\tau) = \lim_{X \to \infty} \frac{1}{2X} \int_{-\infty}^{\infty} y(x)\, y(x+\tau)\, dx \qquad (2.3)$$

The autocorrelation function has the symmetrical property $R_Y(\tau) = R_Y(-\tau)$. It is to be noted that the spectral density is a non-negative quantity. The autocorrelation and the power spectral density functions form a Fourier transform pair and are related as follows:

$$\phi_Y(\Omega) = \frac{1}{2\pi} \int_{-\infty}^{\infty} R_Y(\tau)\, e^{-i\Omega\tau}\, d\tau \qquad (2.4a)$$

$$R_Y(\tau) = \int_{-\infty}^{\infty} \phi_Y(\Omega)\, e^{i\Omega\tau}\, d\Omega \qquad (2.4b)$$

It can be shown, from Eqs. (2.3) and (2.4b), that

$$\sigma^2 = \overline{y^2}(x) = R_Y(0) = \int_0^\infty \phi_Y(\Omega)\, d\Omega \qquad (2.5)$$

where σ is the root-mean-square value (or standard deviation) of the disturbance function, $y(x)$, and is a convenient measure for comparison of the overall roughness of the runways.

The evaluation of the power spectra can be done through 'data processing' - digital and analog - procedures. Details of measurement and analysis of random data and data processing procedures are given elsewhere[2,3]. In the present work, digital technique of data processing was used to evaluate the spectral density. The digital technique consists in digitizing a continuous record or data into discrete numbers and evaluating the spectral density through numerical calculations on digital computers. In digitizing, the sampling interval h is chosen such that

$$h = \frac{1}{2f_c} \qquad (2.6)$$

where f_c is the cutoff frequency. f_c is also called the 'Nyquist frequency'[2]. The choice of h must be small enough so that 'aliasing'[2] is not a problem. This aliasing is a source of error in which the frequencies higher than 1/2h will get folded into the lower frequencies in the range from 0 to 1/2h.

The aliasing will also confuse the data in the lower frequency range.

In the case of the continuous data of the runway irregularities obtained from profile follower measurements, the runway heights, y(x), were read off at 0.65 ft. interval, over a certain datum, giving a cutoff frequency, f_c, of 0.7692 cycle per ~~ft.~~ sec. or 4.8332 radians per ft. For a runway length of 1600 ft. this sampling interval (h = 0.65 ft.) gave a sample size, N, of 2462 sample points. In surveying the sampling interval was 2 ft. giving for 1600-ft. runway a sample size of 800 points. The cutoff frequency in this case was 0.25 cycle per ft. or 1.571 radians per ft.

The actual steps involved in the numerical calculations of the power spectra are as follows:

2.3.1. Autocorrelation Functions

For N data values $\left\{y'_n\right\}$, n = 1, 2, ..., N, the autocorrelation function, R_r, at the displacement rh is calculated from the Eq. (2.3).

$$R_r \doteq R_y(rh) = \frac{1}{N-r} \sum_{n=1}^{N-r} y'_n \, y'_{n+r} \qquad r = 0,1,2,\ldots,m \tag{2.7}$$

where r is the lag number, m is the maximum lag number, and y'_n is the runway height at a point r, measured over a certain

mean. In case of profile follower measurement, y_n' was calculated from the following relation:

$$y_n' = y_n - \frac{1}{N} \sum_{n=1}^{N} y_n \qquad n = 1,2,\ldots,N \qquad (2.8)$$

where y_n is the runway height read off over a datum at a point n. The second term on the right hand side of Eq. (2.8) denotes the mean of $\{y_n\}$, $n = 1,2,\ldots,N$.

In the case of survey measurements, it was desirable to make some modifications to the actual measured profile, because the runway heights exhibited large changes in elevations at very long wavelengths. These large changes at low frequencies have a tendency to complicate and distort power estimates at high frequencies because of the effective filter characteristics of the numerical estimators. One way of avoiding these adverse effects is by 'prefiltering' or 'prewhitening' the original data. The filter used in the present case is a high pass digital filter defined by

$$y'(x) = y(x) - y(x - h) \qquad (2.9)$$

where $y'(x)$ is the prewhitened runway height to be used in Eq. (2.7) for autocorrelation function estimates, $y(x)$ is the original runway height measured over a datum and h is the interval between successive values of y. The above linear

operation (2.9) corresponds to the multiplication in the frequency plane by the function

$$F(\Omega) = 1 - e^{-i\Omega h}$$

where Ω is the spatial frequency in radians per ft.

The maximum lag number, m, is chosen such that it is less than one-tenth the sample size N - a thumb rule. In the present investigation m chosen was 40.

2.3.2. Power Spectral Density Functions

(i) The initial or 'raw' estimates of the power spectral density function are calculated from the following numerical form of Eq. (2.4a)

$$\phi_k = \phi\left(\frac{\pi k}{mh}\right) = \frac{h}{\pi}\left[R_0 + 2\sum_{r=1}^{m-1} R_r \cos\left(\frac{\pi r k}{m}\right) + (-1)^k R_m \right]$$

$$k = 0,1,2,\ldots,m \qquad (2.10)$$

where $\phi_k = \phi(\Omega)$; $\Omega = \frac{\pi k}{mh}$ $k = 0,1,2,\ldots,m$.

$\Omega = \frac{\pi}{h}$ corresponds to the cutoff frequency.

(ii) Final 'smooth' estimates of the power spectral density are determined as follows:

$$\phi'_0 = \frac{1}{2}\phi_0 + \frac{1}{2}\phi_1$$

$$\phi'_k = \frac{1}{4}\phi_{k-1} + \frac{1}{2}\phi_k + \frac{1}{4}\phi_{k+1} \quad k = 1,2,\ldots,m$$

$$\phi_m = \frac{1}{2}\phi_{m-1} + \frac{1}{2}\phi_m \qquad (2.11)$$

In the case of power spectra calculations for survey data, the final smooth power estimates are divided by

$$|F(\Omega)|^2 = 2(1 - \cos\Omega h)$$

in order to compensate for the prewhitening operation.

Smooth estimates of power spectral density functions for both the data obtained from survey as well as profilometer measurements were made with the help of IBM 7044 digital computer. Power spectral density functions are plotted against spatial frequency and are as shown in Fig. 2.5.

2.3.3. Results

In Fig. 2.5, the power spectral density function for survey data (curve 1) is plotted between frequencies 0.0393 and 1.571 radians per ft. corresponding to wavelengths between 160 and 4 ft., and that for profilometer data (curve 2) is plotted between frequencies 0.1208 and 4.8332 radians per ft. corresponding to wavelengths between 52 and 1.3 ft. It is seen

from these curves that the power estimates from survey data are good for longer wavelengths and that from profilometer data are good for smaller wavelengths. Though the runway selected for two types of roughness measurement was same, the values of the spectral density, estimated separately for each type of measurement, seem to agree in the frequency range of 0.9 and 1.57 radians per ft. The explanation for the nonagreement of values at lower frequencies is obvious from the limitations of profile follower measurement, mentioned in Section 2.2.5. If a slope correction is applied to the data obtained from profile follower measurement considering the attitude of the vehicle and the follower wheel on the runway, it may be possible then that curves 1 and 2 (Fig. 2.5) will agree well in all frequency ranges. It can be seen from Fig. 2.5 that curves 1 and 2 together provide a realistic power spectral density curve over the entire frequency range. This combined PSD curve is found to agree well with the mean PSD curve[15] (curve 3).

CHAPTER 3

LUMPED PARAMETER MODEL OF AN AIRCRAFT

3.1 Introduction

The principal structural components of an aircraft are:

(i) Wings

(ii) Fuselage

(iii) Tail surfaces and

(iv) Landing gear.

The mass and stiffness of the aircraft is distributed over each of these components which are elastically interconnected. A dynamic analysis of such a system based on actual mass and stiffness distribution is extremely difficult and complicated. Therefore, an idealized mathematical model seems necessary to deal easily with such problems. In this study a typical small aircraft with truss-type undercarriage (Fig. 3.1) is idealized to a lumped parameter model shown in Fig. 3.2. In arriving at the idealized model, the undercarriage is kept as it is, but the half-wings and fuselage (with tail plane) are replaced by 'equivalent' masses and stiffnesses.

In this chapter, methods of finding the equivalent mass and equivalent stiffness for discrete and continuous systems are described. It is also shown how the idealized model shown in Fig. 3.2 is arrived at.

3.2. 'Equivalent' Mass and Stiffness

The motivation behind finding the 'equivalent' masses and stiffnesses (or springs) is the following:

It is difficult, sometimes, to deal with certain systems having many or infinite number of degrees of freedom. From finding the equivalent quantities, such as equivalent mass, spring, and applied force, such systems can be reduced to systems having one or any convenient number of degrees of freedom. The advantage in finding equivalent quantities is that the analysis of the reduced systems can be carried out more easily and conveniently by certain known available methods. The equivalent mass and spring are found by equating the energy stored in the equivalent system to the total energy stored in the original system.

Williams[5] has given a full description of finding the equivalent quantities in his book. The procedure for finding equivalent mass and equivalent spring for a discrete system having n degrees of freedom and for a continuous system is given below. The same procedure has been applied in the present study to find the equivalent mass and stiffness of the half-wings and the fuselage and tail plane.

3.2.1. Discrete System

Example: A Spring-Mass System

Consider a system having n masses, $m_1, m_2, \ldots, m_n$,

connected by n springs of stiffnesses $k_1, k_2, \ldots, k_n$, as shown in Fig. 3.3(a). Coordinates $x_1, x_2, \ldots, x_n$ represent the displacements of the masses $m_1, m_2, \ldots, m_n$ respectively, the motion being restricted to the straight line through the masses. Suppose the equivalent mass and spring for this system are required, which essentially means finding an 'equivalent' system having one degree of freedom. The simplification in reducing degrees of freedom from n to one consists in replacing the mass elements of the system by an 'equivalent mass' and the springs by an 'equivalent spring' at the station chosen arbitrarily for the equivalent mass. Once the equivalent system is found, standard solution can be applied directly.

Let the mode shape of the system be defined by ratios r. These ratios define the relative displacement of every mass in terms of the relative displacement of any two chosen masses. Let the motion of m_2 relative to m_1 be chosen as the basic displacement. Then we have

$$\begin{aligned} x_3 - x_1 &= r_3(x_2 - x_1), \\ x_4 - x_1 &= r_4(x_2 - x_1), \\ &\cdots\cdots\cdots \\ &\cdots\cdots\cdots \\ x_n - x_1 &= r_n(x_2 - x_1). \end{aligned} \qquad (3.1)$$

If the system is oscillating freely with its centre

of gravity at rest and without any external forces, the sum of inertia forces is then zero. Therefore,

$$m_1\ddot{x}_1 + m_2\ddot{x}_2 + \ldots + m_n\ddot{x}_n = 0 \qquad (3.2)$$

Since, in the condition of steady oscillation in simple harmonic motion, the accelerations are directly proportional to the displacements, Eq. (3.2) can be written as

$$m_1x_1 + m_2x_2 + \ldots + m_nx_n = 0 \qquad (3.3)$$

Using relations (3.1), Eq. (3.3) can be written as

$$m_1x_1 + m_2x_2 + m_3[\, x_1 + r_3(x_2-x_1)\,] + \ldots + m_n[\, x_1 + r_n(x_2-x_1)\,] = 0$$

or

$$x_1(m_1 + m_2 + \ldots + m_n) = -(x_2-x_1)(m_2 + m_3r_3 + \ldots + m_nr_n)$$

or

$$x_1 = -\alpha(x_2-x_1) \qquad (3.4)$$

where

$$\alpha = \frac{m_2 + m_3r_3 + \ldots + m_nr_n}{m_1 + m_2 + \ldots + m_n} \qquad (3.5)$$

By making use of relations (3.1) and (3.4) the displacements of all the masses can be expressed in terms of the displacement of any one mass, such as x_1 of m_1. Thus,

$$
\begin{aligned}
x_2 &= (1 - \frac{1}{\alpha})x_1 = R_2 x_1 \text{ (say)}, \\
x_3 &= (1 - \frac{r_3}{\alpha})x_1 = R_3 x_1, \\
&\cdots\cdots\cdots\cdots \\
&\cdots\cdots\cdots\cdots \\
x_n &= (1 - \frac{r_n}{\alpha})x_1 = R_n x_1
\end{aligned}
\qquad (3.6)
$$

where α is given by (3.5).

Equivalent Mass: The equivalent mass, M, at station 1 can now be readily found by equating the kinetic energy of the equivalent mass to the sum of the kinetic energies of the individual masses. On this basis, we have

$$\frac{1}{2} M\dot{x}_1^2 = \frac{1}{2}(m_1\dot{x}_1^2 + m_2\dot{x}_2^2 + m_3\dot{x}_3^2 + \ldots + m_n\dot{x}_n^2)$$

which, by relations (3.6) becomes

$$\frac{1}{2}M\dot{x}_1^2 = \frac{1}{2}\dot{x}_1^2(m_1 + m_2R_2^2 + m_3R_3^2 + \ldots + m_nR_n^2)$$

which gives the equivalent mass at station 1 as

$$M = m_1 + m_2R_2^2 + m_3R_3^2 + \ldots + m_nR_n^2 \qquad (3.7)$$

Equivalent Spring or Stiffness: The principle made use of in finding the equivalent stiffness is that the same energy is stored in the equivalent spring as that stored in all the spring

of the system for the same reference displacement, such as x_1. Thus, the equivalent stiffness, K, is given by

$$\frac{1}{2} Kx_1^2 = \frac{1}{2}[k_1x_1^2 + k_2(x_2-x_1)^2 + k_3(x_3-x_2)^2 + \ldots + k_n(x_n-x_{n-1})^2]$$

This, after using relations (3.6), can be written as

$$\frac{1}{2} Kx_1^2 = \frac{1}{2} x_1^2[k_1 + k_2(R_2-1)^2 + k_3(R_3-R_2)^2 + \ldots + k_n(R_n-R_{n-1})^2]$$

which gives the equivalent stiffness at station 1 as

$$K = k_1 + k_2(R_2-1)^2 + k_3(R_3-R_2)^2 + \ldots + k_n(R_n-R_{n-1})^2 \qquad (3.8)$$

The equivalent system of the present case is shown in Fig. 3.3(b).

3.2.2. Equivalent Spring-Mass System for a System With Infinite Number of Degrees of Freedom

Example: A Cantilever (Fig.3.4)

In reducing the cantilever (with infinite number of degrees of freedom) to a single-degree-of-freedom system, we have to choose a particular shape for the deflection curve (i.e. the mode shape), so that the deflection everywhere is defined by the deflection at any one point, such as the deflection y_0 at the tip, as shown in Fig. 3.4.

Let the free end of the cantilever be the 'reference section' where we want to locate the equivalent mass. If the (variable) mass per unit length is m, the kinetic energy of an element dx of the cantilever at x is

$$\delta T = \frac{1}{2} (m\, dx)\, \dot{y}^2$$

$$= \frac{1}{2} m \dot{y}_0^2 (\eta_x)^2\, dx$$

where $$\eta_x = \frac{\dot{y}}{\dot{y}_0} = \frac{y}{y_0} \qquad (3.9)$$

The total kinetic energy is

$$T = \int \delta T = \frac{1}{2} \dot{y}_0^2 \int_0^l m(\eta_x)^2\, dx,$$

which should be equal to the kinetic energy of the equivalent mass M. Thus,

$$\frac{1}{2} M \dot{y}_0^2 = \frac{1}{2} \dot{y}_0^2 \int_0^l m(\eta_x)^2\, dx$$

which gives

$$M = \int_0^l m(\eta_x)^2\, dx \qquad (3.10)$$

The equivalent spring constant, K, is found by equating the energy stored in the spring under a displacement y_0 to the total strain energy of the cantilever. Thus,

$$\frac{1}{2} K y_0^2 = \frac{1}{2} E \int_0^l I \left(\frac{d^2y}{dx^2}\right)^2 dx$$

which gives

$$K = E \int_0^l I\left(\frac{d^2y}{dx^2}\right)^2 dx \qquad (3.11)$$

where E = Young's modulus, and

I = (Variable) moment of inertia.

It is to be noted that, if the displacement curve (mode shape) and the corresponding frequency of vibration are determined, then we need calculate only one of the equivalent quantities, M or K, as one can be found out from the other usingthe relation

$$\omega^2 = \frac{K}{M} \qquad (3.12)$$

where ω is the circular frequency of vibration.

3.3. Lumped Parameter Model of the Aircraft Shown in Fig. 3.1

In idealizing the aircraft to a lumped parameter system, the undercarriage is kept unaltered, but the wing, the fuselage (along with tail plane) and the landing wheels are replaced by equivalent masses. The half-wings are replaced by the equivalent masses m_1 and m_5 ($m_1 = m_5$) and the massless members 1 and 12 of equivalent stiffness K_e each, as shown in Fig. 3.2. The fuselage with tail plane is replaced by the equivalent mass m_3 at the centre of gravity. The main landing

wheels are replaced by the equivalent masses m_2 and m_4 ($m_2 = m_4$). The tyres are replaced by springs of stiffness k each as shown in the figure.

Eqs.(3.10) and (3.12) are made use of in calculating the equivalent mass and stiffness for the wing. The equivalent quantities are calculated for the fundamental mode, considering half wing as a cantilever. The equivalent mass is located at a station 116 inches from the wing root. With an average weight distribution of 12 lbs./ft. run and average moment of inertia of 60 $in.^4$, the equivalent mass, m_1, and the equivalent stiffness, K_e, for the wing are calculated to be 0.4 $lb.-sec.^2/in.$ and 1319 lbs./in. respectively. To find the value of equivalent masses for the landing wheels, each wheel together with undercarriage members is assumed to weigh 20 lbs., giving $m_2 = m_4 = 0.052$ $lb.-sec.^2/in.$ The value of m_3 (for fuselage and tail plane) is taken from the all up weight of the aircraft (1750 lbs.) minus the values of m_1, m_2, m_4, m_5. The calculated value of m_3 is 3.63 $lbs.-sec.^2/in.$

The value of the spring constant (tyre stiffness) to be used for the landing wheels depends on the tyre pressure. Tyre stiffness test at different tyre pressures was conducted for an airplane landing wheel having Dunlop tyre - 26" x 7.75" - 13" - 8 ply rating. The wheel was loaded vertically in a universal testing machine and compression of tyre at different

loads was noted. The load-deflection curves for the tyre at different tyre pressures were drawn and are as shown in Fig. 3.6. From these curves the value of tyre stiffness can be obtained. However, these curves could not be made use of in the present work as the airplane under consideration had an entirely different wheel. Tyre stiffness of 400, 600, 800 lbs./in. will be used in the analysis and its effect on the airplane response will be studied.

The idealized model shown in Fig. 3.2 is a symmetric structure with masses m_1, m_2, m_3, m_4 and m_5 interconnected by members numbered from 1 to 12. The undercarriage forms a space structure and consists of members from 2 to 11. Coordinates X, Y and Z determine the geometry of the structure. The generalized coordinate system for the dynamic model is denoted by coordinates z_1, z_2, z_3, z_4 and z_5. The following assumptions will be made for simplicity in the forthcoming analysis.

1) Members 1 and 12 are bending members and all other members (2 to 11) are truss members.
2) All joints, except B and N, are pin-joints.
3) Joints A and M are assumed to lie on the elastic axis of the wing so that torsional effects are absent.
4) Members 3 to 10 are of hollow round cross-section and members 2 and 11 are of airfoil cross-section.

5) The motion of the aircraft is considered only in the vertical direction (Z-direction) and thus the dynamic model has only five degrees of freedom.

The values of various parameters which will be used in the response calculations are given in Table 3.1.

CHAPTER 4

RESPONSE OF AIRCRAFT TO RUNWAY ROUGHNESS

4.1. Introduction

During taxiing, take-off and landing an aircraft is subjected to random excitation due to the runway roughness. The prediction of the aircraft response, such as stresses in the airframe, vertical displacement and acceleration at the c.g. of the aircraft or at the pilot's position, etc., to such excitation is of interest. The response can be determined either experimentally or analytically. In the present investigation, the response of a light airplane to runway roughness during taxiing is determined analytically for an idealized model (Fig.3.2) of the airplane through random vibration approach. In applying this approach, the system is assumed to be linear and the excitation stationary. However, when the system is nonlinear (nonlinearity comes mainly from landing gear system) the analytical approach becomes too difficult. Response parameters of interest are: the stresses developed in the undercarriage members and the vertical acceleration at the pilot's portion. These responses are computed for different constant taxiing speeds and are presented in terms of standard deviation or the root-mean-square (r.m.s.) value. Ground excitation during take-off is a non-stationary random process.

Response during take-off at constant acceleration is computed by numerical integration of the equation of motion. In calculating the response, the lift forces acting on the airplane are not considered, and input to both landing gears are assumed to be same. This chapter deals with the analytical procedures for finding the response of the airplane to random excitation.

4.2. Response During Taxiing

An aircraft taxiing at constant speed on a runway having a stationary random roughness is subjected to a stationary excitation. Hence, the mean square response of the airplane can be conveniently determined by frequency domain approach which makes use of the power spectral density functions of the excitation.

4.2.1. Equations of Motion

The system considered for response calculations is the lumped parameter model shown in Fig. 3.2. Five degrees of freedom considered are defined by the generalized coordinates z_1, z_2, z_3, z_4 and z_5. The size of the stiffness matrix for the system will be 5 x 5. To get this stiffness matrix, an additional degress of freedom at joint G, defined by z_6 where no inertia force acts, will be introduced which gives rise to a 6 x 6 stiffness matrix. Eliminating z_6 from the equations of

motion will result in 5 x 5 stiffness matrix. The undamped equations of motion of the system considering z_6 also, can be written in the matrix form as

$$M\ddot{Z} + K\,(Z - y) = 0 \tag{4.1}$$

where

$$M = \begin{bmatrix} m_1 & & & & & 0 \\ & m_2 & & & & \\ & & m_3 & & & \\ & & & m_4 & & \\ & & & & m_5 & \\ 0 & & & & & 0 \end{bmatrix} \tag{4.2}$$

$$K = \begin{bmatrix} k_{11} & k_{12} & k_{13} & k_{14} & k_{15} & k_{16} \\ k_{21} & k_{22} & k_{23} & k_{24} & k_{25} & k_{26} \\ k_{31} & k_{32} & k_{33} & k_{34} & k_{35} & k_{36} \\ k_{41} & k_{42} & k_{43} & k_{44} & k_{45} & k_{46} \\ k_{51} & k_{52} & k_{53} & k_{54} & k_{55} & k_{56} \\ k_{61} & k_{62} & k_{63} & k_{64} & k_{65} & k_{66} \end{bmatrix} \tag{4.3}$$

$$Z = \begin{Bmatrix} z_1 \\ z_2 \\ z_3 \\ z_4 \\ z_5 \\ z_6 \end{Bmatrix} \tag{4.4}$$

y is the base displacement and $(\ddot{\ })$ denotes second time-derivative.

Now, to find the total stiffness matrix, K, the following relation will be made use of.

$$K = T^T K' T \tag{4.5}$$

where T is the transformation matrix containing the direction cosines of the members of the structure referred to coordinates $z_1, z_2, \ldots, z_6$, T^T is transposed matrix of T and K' is a diagonal matrix containing stiffness of individual members. Referring to Fig. 3.2, T can be readily written as

$$T = \begin{array}{c} \text{Member No.} \\ 1 \\ 2 \\ 3 \\ 4 \\ 5 \\ 6 \\ 7 \\ 8 \\ 9 \\ 10 \\ 11 \\ 12 \\ 13 \\ 14 \end{array} \begin{array}{c} \begin{array}{cccccc} z_1 & z_2 & z_3 & z_4 & z_5 & z_6 \end{array} \\ \begin{bmatrix} 1 & 0 & -1 & 0 & 0 & 0 \\ -h_1/L_2 & 0 & h_1/L_2 & 0 & 0 & 0 \\ 0 & h_4/L_3 & -h_4/L_3 & 0 & 0 & 0 \\ 0 & h_4/L_4 & -h_4/L_4 & 0 & 0 & 0 \\ 0 & 0 & -h_2/L_5 & 0 & 0 & h_2/L_5 \\ 0 & h_3/L_6 & 0 & 0 & 0 & -h_3/L_6 \\ 0 & 0 & 0 & h_3/L_7 & 0 & -h_3/L_7 \\ 0 & 0 & -h_2/L_8 & 0 & 0 & h_2/L_8 \\ 0 & 0 & -h_4/L_9 & h_4/L_9 & 0 & 0 \\ 0 & 0 & -h_4/L_{10} & h_4/L_{10} & 0 & 0 \\ 0 & 0 & h_1/L_{11} & 0 & -h_1/L_{11} & 0 \\ 0 & 0 & 1 & 0 & -1 & 0 \\ 0 & -1 & 0 & 0 & 0 & 0 \\ 0 & 0 & 0 & -1 & 0 & 0 \end{bmatrix} \end{array} \tag{4.6}$$

where L_2, L_3, ..., L_{11} are the lengths of the members 2, 3, .., 11 respectively, $h_4 = (h_2 + h_3)$ and h_1, h_2, h_3, which determine the z-ordinate of the members, are as indicated in Fig. 3.2. It is to be noted that in writing the direction cosines, members 1 and 12 are considered as bending members and members 13 and 14 as springs. The stiffness matrix, K', is given by

$$K' = \begin{bmatrix} K_e & & & & & & & & & & & & \\ & \frac{A_2E}{L_2} & & & & & & & & & & & \\ & & \frac{A_3E}{L_3} & & & & & & & & & & \\ & & & \frac{A_4E}{L_4} & & & & & & & & & \\ & & & & \frac{A_4E}{L_5} & & & & & & & & \\ & & & & & \frac{A_6E}{L_6} & & & & & & & \\ & & & & & & \frac{A_7E}{L_7} & & & & & & \\ & & & & & & & \frac{A_8E}{L_8} & & & & & \\ & & & & & & & & \frac{A_9E}{L_9} & & & & \\ & & & & & & & & & \frac{A_{10}E}{L_{10}} & & & \\ & & & & & & & & & & \frac{A_{11}E}{L_{11}} & & \\ & & & & & & & & & & & K_e & \\ & & & & & & & & & & & & k \\ & & & & & & & & & & & & & k \end{bmatrix} \qquad (4.7)$$

where K_e = equivalent stiffness of half-wing (stiffness of members 1 and 12),

E = Young's modulus of elasticity,

k = tyre stiffness (stiffness of members 13 and 14)

and A_2, A_3,..., A_{11} are areas of cross-section of the members 2, 3,..., 11 respectively.

Substituting for T^T, K' and T in Eq. (4.8) and simplifying the elements k_{11}, k_{12}, etc., of the total stiffness matrix are found and they are as follows:

$$k_{11} = K_e + A_2 E h_1^2 / L_2^3$$

$$k_{22} = E[\, h_4^2 (A_3/L_3^3 + A_4/L_4^3) + A_6 h_3^2 / L_6^3 \,] + k$$

$$k_{33} = 2K_e + E[\, h_1^2 (A_2/L_2^3 + A_{11}/L_{11}^3) + h_2^2 (A_5/L_5^3 + A_8/L_8^3) + h_4^2 (A_3/L_3^3 + A_4/L_4^3 + A_9/L_9^3 + A_{10}/L_{10}^3) \,]$$

$$k_{44} = E[\, A_7 h_3^2 / L_7^3 + h_4^2 (A_9/L_9^3 + A_{10}/L_{10}^3) \,],$$

$$k_{55} = K_e + A_{11} h_1^2 / L_{11}^3$$

$$k_{66} = E[\, h_2^2 (A_5/L_5^3 + A_8/L_8^3) + h_3^2 (A_6/L_6^3 + A_7/L_7^3) \,]$$

$$k_{13} = k_{31} = - k_{11}$$

$$k_{23} = k_{32} = - Eh_4^2(A_3/L_3^3 + A_4/L_4^3)$$

$$k_{26} = k_{62} = - EA_6h_3^2/L_6^3$$

$$k_{34} = k_{43} = - Eh_4^2(A_9/L_9^3 + A_{10}/L_{10}^3)$$

$$k_{36} = k_{63} = - Eh_2^2(A_5/L_5^3 + A_8/L_8^3)$$

$$k_{35} = k_{53} = - k_{55}$$

$$k_{46} = k_{64} = - EA_7h_3^2/L_7^3 \qquad (4.8)$$

and all other elements are zero.

Eq. (4.1) is now rewritten as

$$-\left\{\begin{array}{c} M^*\ddot{Z}^* \\ \hline 0 \end{array}\right\} = \left[\begin{array}{c|c} K_{11} & K_{12} \\ \hline K_{21} & K_{22} \end{array}\right] \left\{\begin{array}{c} Z^*-y \\ \hline z_6-y \end{array}\right\} \qquad (4.9)$$

where

$$M^* = \begin{bmatrix} m_1 & & & & 0 \\ & m2 & & & \\ & & m3 & & \\ & & & m_4 & \\ 0 & & & & m_5 \end{bmatrix}, \quad Z^* = \begin{Bmatrix} z_1 \\ z_2 \\ z_3 \\ z_4 \\ z_5 \end{Bmatrix} \qquad (4.10)$$

and K_{11}, K_{12}, K_{21}, and K_{22} are partitioned matrices of K.

Eq. (4.9) is equivalent to the two following equations.

$$
\begin{aligned}
-M^* \ddot{Z}^* &= K_{11}(Z^* - y) + K_{12}(z_6 - y) \\
0 &= K_{21}(Z^* - y) + K_{22}(z_6 - y)
\end{aligned}
\tag{4.11}
$$

The second of these equations is solved for z_6 and substituted into the first to give the reduced form

$$-M^* \ddot{Z}^* = K^*(Z^* - y)$$

where

$$K^* = K_{11} - K_{12} K_{22}^{-1} K_{21} \tag{4.12}$$

is a 5 x 5 matrix and its elements are given by

$$
\begin{aligned}
k_{11}^* &= k_{11} \\
k_{22}^* &= k_{22} - k_{26}^2/k_{66} \\
k_{33}^* &= k_{33} - k_{36}^2/k_{66} \\
k_{44}^* &= k_{44} - k_{46}^2/k_{66} \\
k_{55}^* &= k_{55} \\
k_{13}^* &= k_{31}^* = -k_{11} \\
k_{23}^* &= k_{32}^* = k_{23} - k_{26}k_{36}/k_{66} \\
k_{24}^* &= k_{42}^* = -k_{26}k_{46}/k_{66} \\
k_{34}^* &= k_{43}^* = k_{34} - k_{36}k_{46}/k_{66} \\
k_{35}^* &= k_{53}^* = k_{35}.
\end{aligned}
$$

All other elements are zero. The equations of motion in the generalized coordinates are given by

$$M^* \ddot{Z}^* + K^* (Z^* - y) = 0 \tag{4.13}$$

Putting

$$X = Z^* - y \tag{4.14}$$

where

$$X = \begin{Bmatrix} x_1 \\ x_2 \\ x_3 \\ x_4 \\ x_5 \end{Bmatrix} \tag{4.15}$$

Eq. (4.13) reduces to

$$M^* \ddot{X} + K^* X = - F(t) \tag{4.16}$$

where

$$F(t) = \begin{Bmatrix} m_1 \\ m_2 \\ m_3 \\ m_4 \\ m_5 \end{Bmatrix} \ddot{y}(t) \tag{4.17}$$

$\ddot{y}(t)$ is the base acceleration.

4.2.2. Damped Uncoupled Equations of Motion

Introducing proportional damping into the system, the equations of motion become

$$M^* \ddot{X} + C \dot{X} + K^* X = - F(t) \qquad (4.18)$$

where C is the damping matrix (5 x 5). These equations are statically coupled. They can be decoupled by making suitable transformations. Let

$$X = M^{*-\frac{1}{2}} X_1 \qquad (4.19)$$

Substituting this transformation into Eq. (4.18) and pre-multiplying by $M^{*-\frac{1}{2}}$, Eq. (4.18) becomes

$$\ddot{X}_1 + A\dot{X}_1 + BX_1 = - M^{*-\frac{1}{2}} F(t) \qquad (4.20)$$

where

$$A = M^{*-1/2} C M^{*-1/2}$$

$$B = M^{*-1/2} K M^{*-1/2}$$

are real, symmetric and positive definite. Under these conditions and the constraint that AB = BA, it can be shown that there exists a transformation

$$X_1 = \theta P \qquad (4.21)$$

such that

$$\theta^T \theta = I \qquad (4.22)$$

$$\theta^T A \theta = [2\beta\omega_i] \quad i = 1,2,\ldots,5 \tag{4.23}$$

$$\theta^T B \theta = [\omega_i^2] \quad i = 1,2,\ldots,5 \tag{4.24}$$

where

$$P = \begin{Bmatrix} p_1 \\ p_2 \\ p_3 \\ p_4 \\ p_5 \end{Bmatrix} \tag{4.25}$$

represents the normal coordinates, θ is the normalized modal column matrix of B, β is the critical damping factor assumed to be constant in all the modes and ω_i is the i^{th} natural frequency of the system. Under these transformations Eq.(4.20) reduces to

$$\ddot{p}_i + 2\beta\omega_i\dot{p}_i + \omega_i^2 p_i = -\Gamma_i \ddot{y}(t) \quad i = 1,2,\ldots,5 \tag{4.26}$$

where Γ_i is the i^{th} modal participation factor obtained by simplifying the triple matrix product $\theta^T M^{*-1/2} F(t)$. The left hand side of Eq. (4.26) can be thought of as representing a single-degree-of-freedom system with natural frequency ω_i. Working back through the transformations, the mode shapes of the system U_1, U_2, U_3, U_4 and U_5, which will be the displacements in the generalized coordinates, can be obtained. Hence

$$X = U P$$

and

$$U = M^{*-1/2}\theta \tag{4.27}$$

where

$$U = [\, U_1 \; U_2 \; U_3 \; U_4 \; U_5 \,] \tag{4.28}$$

and

$$U_1 = \begin{Bmatrix} u_{11} \\ u_{21} \\ u_{31} \\ u_{41} \\ u_{51} \end{Bmatrix}, U_2 = \begin{Bmatrix} u_{12} \\ u_{22} \\ u_{32} \\ u_{42} \\ u_{52} \end{Bmatrix}, U_3 = \begin{Bmatrix} u_{13} \\ u_{23} \\ u_{33} \\ u_{43} \\ u_{53} \end{Bmatrix}, U_4 = \begin{Bmatrix} u_{14} \\ u_{24} \\ u_{34} \\ u_{44} \\ u_{54} \end{Bmatrix}, U_5 = \begin{Bmatrix} u_{15} \\ u_{25} \\ u_{35} \\ u_{45} \\ u_{55} \end{Bmatrix} \tag{4.29}$$

are the mode shapes.

4.2.3. Response Calculations

If for $\ddot{y}(t)$ a simple harmonic forcing function $\ddot{y}(t) = e^{i\omega t}$ is substituted, then the steady-state solution of Eq. (4.26) is given by

$$p_i(t) = \frac{\sqrt{i}}{\omega_i^2} H_i(\omega)\, \ddot{y}(t) \tag{4.30}$$

where

$$H_i(\omega) = \frac{-1}{1-(\omega/\omega_i)^2 + j2\beta\omega/\omega_i} \qquad i = i,2,\ldots 5 \tag{4.31}$$

where again $j = \sqrt{-1}$. $H_i(\omega)$ is the frequency response function of the (linear) system.

The relative displacements of the masses in the generalized coordinates are related to the displacements in the normal coordinates by the Eq. (4.27) which can be rewritten as

$$x_i = \sum_{j=1}^{5} u_{ij} p_j \tag{4.32}$$

These displacements are treated as random variables and the covariant matrix of the relative displacement vector X, which contains the cross products, can be shown to be given by[6,7]

$$\text{cov}\ (x_k x_l) = \sum_{i=1}^{5} \sum_{j=1}^{5} u_{ki}\, u_{lj} \frac{\Gamma_i \Gamma_j}{\omega_i^2 \omega_j^2} \frac{1}{2\pi} \int_0^{\infty} |H_i(\omega)|\, |H_j(\omega)|\, \phi_{\ddot{Y}\ddot{Y}}(\omega)\, d\omega$$

$$k = 1, 2, \ldots, 5$$

$$l = 1, 2, \ldots, 5 \tag{4.33}$$

where

$$|H_i(\omega)| = \left[\left\{ 1 - (\omega/\omega_i)^2 \right\}^2 + (2\beta\omega/\omega_i)^2 \right]^{-1/2} \tag{4.34}$$

and $\phi_{\ddot{Y}\ddot{Y}}(\omega)$ is the power spectral density function of the excitation, $\ddot{y}(t)$.

4.2.4. Approximate Solution

For a lightly damped system, $|H_i(\omega)|$ given by

Eq. (4.34) have regions of pronounced peaks in the neighbourhood of the corresponding natural frequencies ω_i. If ω_i and ω_j are well separated, the products $|H_i(\omega)||H_j(\omega)|$ for $i \neq j$ are seen to be small in comparison with the same products for $i = j$. Also, terms with $i \neq j$ in Eq. (4.33) may be negative or positive depending upon the sign of the product $u_{ki}\ u_{lj}\ \Gamma_i \Gamma_j$ while terms with $i=j$ are always positive. With these approximations, Eq. (4.33) may be written as

$$\text{cov}(x_k x_l) = \sum_{i=1}^{5} u_{ki}\ u_{li}\ \frac{\Gamma_i^2}{2\pi\omega_i^2} \int_0^\infty |H_i(\omega)|^2\ \phi_{YY}(\omega)\ d\omega$$

$$k = 1,2,\ldots,5$$

$$l = 1,2,\ldots,5 \qquad (4.35)$$

If the $\phi_Y^{\cdot\cdot}(\omega)$ curve is flat around ω_i, then white noise assumption can be made and the integrals of Eq. (4.35) for a lightly damped system can be approximated by replacing $\phi_Y^{\cdot\cdot}(\omega)$ by its discrete values at the natural frequencies ω_i [6,7]. Thus Eq. (4.35) reduces to

$$\text{cov}(x_k x_l) = \sum_{i=1}^{5} u_{ki}\ u_{li}\ \frac{\Gamma_i^2}{\omega_i^3}\ \frac{\phi_Y^{\cdot\cdot}(\omega_i)}{8\beta} \qquad (4.36)$$

$$k = 1,2,\ldots,5$$

$$l = 1,2,\ldots,5$$

In particular,

$$\text{cov}(\dot{x}_k x_k) = \sigma^2_{\dot{x}_k} = \sum_{i=1}^{5} u^3_{ki} \frac{\Gamma_i^2}{\omega_i^3} \frac{\phi_{\ddot{Y}}(\omega_i)}{8\beta}$$

$$k = 1,2,\ldots,5 \qquad (4.37)$$

where $\sigma^2_{\dot{x}_k}$ is the mean square value of the response.

4.2.5. Power Spectral Density of Excitation

The spectral density, $\phi_{\ddot{Y}}(\omega)$, of the excitation to be used in Eq. (4.35) should be in acceleration units like $(\text{ft.}^2/\text{sec.}^4)/(\text{rad./sec.})$. $\phi_{\ddot{Y}}(\omega)$ can be obtained from the power spectral density functions of the runway roughness in the following way.

Let $\phi_Y(\Omega)$ be the spectral density of the runway roughness which is in $\text{ft.}^2/(\text{rad./ft.})$ units. An airplane taxiing at a constant velocity V(ft./sec.) senses an excitation of spectral density $\phi_Y(\omega)$ in $\text{ft.}^2/(\text{rad./sec.})$ units, given by

$$\phi_Y(\omega) = \phi_Y(\Omega)/V \qquad (4.38)$$

where

$$\omega = \Omega V \qquad (4.39)$$

is in rad./sec. and Ω in rad./ft. It can be proved from first principles that

$$\phi_{\ddot{Y}}(\omega) = \omega^4 \, \phi_Y(\omega) \tag{4.40}$$

$$\text{i.e.} \quad \phi_{\ddot{Y}}(\omega) = (V\Omega)^4 \, [\, \phi_Y(\Omega)/V \,] \tag{4.41}$$

Thus, from spectral density of the runway roughness spectral density of the excitation an airplane senses when taxiing at a constant velocity can be found. From the combined spectral density curves 1 and 2 for the runway roughness shown in Fig. 2.5, the power spectral density functions, $\phi_{\ddot{Y}}(\omega)$, of the base acceleration were computed for different constant velocities using Eq. (4.41). The curves of $\phi_{\ddot{Y}}(\omega)$ plotted against ω are as shown in Fig. 4.1.

4.2.6. Standard Deviation or r.m.s. Value of Relative Displacement of Masses

The covariant matrix, cov(X), of the relative displacements in the generalized coordinates is a symmetric matrix containing the mean square value of the displacements on its diagonal. The square root of the diagonal elements of cov(X) gives the standard deviation of the relative displacements of masses $m_1, m_2, \ldots, m_5$.

4.2.7. Standard Deviation of Absolute Acceleration of Masses

The absolute acceleration, $\ddot{Z}$, of different masses

of the system is given by

$$\ddot{Z} = \ddot{X} + \ddot{y}(t) \tag{4.42}$$

Using Eq. (4.27), Eq. (4.42) can be written as

$$\ddot{Z} = M^{*-1/2}\,\theta\,\ddot{P} + \ddot{y}(t) \tag{4.43}$$

Using Eq. (4.22), (4.43) can be written as

$$\ddot{Z} = M^{*-1/2}\,\theta\,\left[\ddot{P} + \theta^{T} M^{*1/2}\,\ddot{y}(t)\right]$$

i.e.

$$\ddot{Z} = U\,\ddot{P}_{A} \tag{4.44}$$

where $\ddot{P}_{A} = \ddot{P} + \theta^{T} M^{*1/2}\,\ddot{y}(t)$ gives the absolute accelerations in the normal coordinates. The mean square value of $\ddot{P}_{A}$ can be approximately shown to be given by

$$\overline{\ddot{p}^{2}_{Ai}} = \frac{\omega_i \Gamma_i^{2} \phi_{\ddot{Y}}(\omega_i)}{8\beta}\,(1 + 4\beta^{2}) \qquad i = 1,2,\ldots,5 \tag{4.45}$$

where $\ddot{p}_{A_i}$ are the elements of $\ddot{P}_{A}$. Neglecting the cross products when the frequencies are well separated and using the orthogonality condition in the normal coordinates that the covariance of $p_{A_i}\ p_{A_j}$ is zero, the mean square value of the absolute acceleration of the masses $m_1, m_2, \ldots, m_5$ is given by

$$\overline{\ddot{z}^{2}_{i}} = \sum_{j=1}^{5} u_{ij}^{2}\ \overline{\ddot{p}^{2}_{A_j}} \qquad i = 1, 2, \ldots, 5 \tag{4.46}$$

the square root of which gives the standard deviation of the absolute acceleration. Incidentally, the absolute acceleration of the mass m_3 (Fig. 3.2) represents the absolute acceleration at the cockpit.

4.2.8. Standard Deviation of Stress in Undercarriage Members

The dynamic stresses induced in the members 2 to 11 (see Fig. 3.2) during taxiing are of prime interest here. Let $\delta_2, \delta_3, \ldots, \delta_{11}$ and $s_2, s_3, \ldots, s_{11}$ be the changes in length and the stresses developed, respectively, in the members 2,3,...,11 and be denoted by

$$\delta = \begin{Bmatrix} \delta_2 \\ \delta_3 \\ \cdot \\ \cdot \\ \cdot \\ \delta_{11} \end{Bmatrix} \tag{4.47}$$

and

$$S = \begin{Bmatrix} s_2 \\ s_3 \\ \cdot \\ \cdot \\ \cdot \\ s_{11} \end{Bmatrix} \tag{4.48}$$

δ is related to the relative displacement vector X by

$$\delta = T X \tag{4.49}$$

where T is the transformation matrix given by Eq. (4.6) after deleting the first and the last three rows. $\delta_2, \delta_3, \ldots, \delta_{11}$ are dependent on each other. The covariant matrix of δ is given by

$$\text{cov}(\delta) = T \, \text{cov}(X) \, T^T \tag{4.50}$$

cov(X) in Eq. (4.50) is a 6x6 symmetric matrix and includes the relative displacement, x_6, at the coordinate z_6. x_6 can be obtained from the last equation of the equations of motion given by Eq. (4.1) as

$$x_6 = z_6 - y = -(k_{61}x_1 + k_{62}x_2 + k_{63}x_3 + k_{64}x_4 + k_{65}x_5)/k_{66} \tag{4.51}$$

The $\text{cov}(x_6 x_i)$, i = 1,2,...,6 can be readily found by using Eq. (4.51) and the $\text{cov}(x_i x_j)$, i, j = 1,2,...,5. Now, the changes in length given by δ are related to the stress matrix by

$$S = K' \delta \tag{4.52}$$

where K' is a diagonal matrix given by

$$K' = \lceil E/L_i \rfloor \qquad i = 2,3,\ldots,11 \qquad (4.53)$$

The covariant matrix of S is given by

$$\text{cov}(S) = K' \text{ cov}(\delta) K' \qquad (4.54)$$

The square root of the diagonal elements of cov(S) gives the standard deviation of the dynamic stresses. These stresses denote the standard deviation of the fluctuation of stresses about the static stresses and may be added to the static stresses to get estimates of maximum dynamic stresses. For example, stress given by $|\mu_S| + 3\sigma_D$ represents an estimate of maximum stress with exceedance probability less than 0.27 percent, where μ_S is the static stress and σ_D is the standard deviation of the dynamic stress.

4.2.9. Results

The natrual frequencies and the mode shapes for the idealized system of 'Piper' airplane have been computed using a standard subroutine in IBM 7044 computer. The values are as shown in Table 4.1. The standard deviation of the absolute acceleration at the cockpit, and the dynamic stresses in the undercarriage members for different taxiing speeds have been computed and the values are as shown in Table 4.2. The probabilities that the dynamic stress will exceed the root mean square value σ_D, $2\sigma_D$ and $3\sigma_D$ are given in Table 4.3

The ratios of the estimated maximum dynamic stress to the static stress have been calculated and are shown in Table 4.4.

The effect of tyre stiffness on the fundamental frequency and the response calculations for the idealized model has been studied. The fundamental frequency and the response are found to increase with the increased value of tyre stiffness. The variation of the fundamental frequency and the absolute acceleration at the cockpit against tyre stiffness has been shown in Table 4.5.

4.3. Response During Take-off

Many practical problems in structural dynamics involve excitations which are nonstationary in character. For example, an airplane experiences nonstationary excitations during take-off and landing. These nonstationary excitations lead to nonstationary responses. In practice, the analysis of such problems involving nonstationary excitations is difficult to deal with. Also, such problems require many field records for estimating the statistical properties of nonstationary random processes. In the present study, the response of an airplane (Piper) to nonstationary input during take-off is determined through a deterministic approach, in which the response is computed by numerical integration of the differential equation of motion. The airplane is assumed to move at constant acceleration 'a' during take-off.

4.3.1. Formulation and Solution of the Problem

The airplane under study is idealized to a single-degree-of-freedom system shown in Fig. 4.2. The mass m is so chosen as to represent the all up weight of the airplane (1750 lb.). The system is assumed to have a natural frequency, ω, equal to the fundamental frequency calculated for the lumped parameter system (13.27 rad./sec.) and a stiffness $k = \omega^2 m$. Introducing viscous damping c, the equation of motion for this idealized system subjected to a base displacement, y(t), is written as

$$m\ddot{z} + c\ (\dot{z} - \dot{y}) + k\ (z - y) = 0 \qquad (4.55)$$

where ($\dot{}$) denotes differential with respect to time. Dividing by m and setting $c = 2\beta\omega m$ and $\omega = \sqrt{k/m}$, Eq. (4.55) can be written as

$$\ddot{z} + 2\beta\omega\dot{z} + \omega^2 z = 2\beta\omega\dot{y} + \omega^2 y \qquad (4.56)$$

where β is the critical damping factor and ω is the natural frequency of vibration of the system.

Assuming that y may be approximated by a segmentally linear function as shown in Fig. 4.3, Eq. (4.56) may be written as

$$\ddot{z} + 2\beta\omega\dot{z} + \omega^2 z = 2\beta\omega\frac{\Delta y_i}{\Delta t_i} + \omega^2\left[\, y_i + \frac{\Delta y_i}{\Delta t_i}\,(t - t_i)\,\right]$$

$$t_i \le t \le t_{i+1} \qquad (4.57)$$

where

$$\Delta y_i = y_{i+1} - y_i$$

and $$\Delta t_i = t_{i+1} - t_i \qquad (4.58)$$

The solution of (4.57), for $t_i \leq t \leq t_{i+1}$ is given by

$$z = e^{-\beta\omega(t-t_i)} \left[C_1 \sin\omega\sqrt{1-\beta^2}(t-t_i) + C_2 \cos\omega\sqrt{1-\beta^2}(t-t_i) \right]$$

$$+ y_i + \frac{\Delta y_i}{\Delta t_i} (t-t_i) \qquad (4.59)$$

in which C_1 and C_2 are the constants of integration. Setting $z = z_i$ and $\dot{z} = \dot{z}_i$ at $t = t_i$ and solving for C_1 and C_2, it can be shown that

$$C_1 = (1/\omega\sqrt{1-\beta^2}) \left[\dot{z}_i + \beta\omega(x_i - y_i) - \Delta y_i/\Delta t_i \right]$$

(4.60)

and $C_2 = x_i - y_i$

Substituting (4.60) for C_1 and C_2 in Eq. (4.59), z and $\dot{z}$ at $t = t_{i+1}$ can be shown to be given by

$$\bar{z}_{i+1} = A(\beta, \omega, \Delta t_i)\, \bar{z}_i + B(\beta, \omega, \Delta t_i)\, \bar{y}_i \qquad (4.61a)$$

in which

$$\bar{z}_{i+1} = \begin{Bmatrix} z_{i+1} \\ \dot{z}_{i+1} \end{Bmatrix} , \quad \bar{z}_i = \begin{Bmatrix} z_i \\ \dot{z}_i \end{Bmatrix} , \quad \bar{y}_i = \begin{Bmatrix} y_i \\ y_{i+1} \end{Bmatrix} \tag{4.61b}$$

$$A = \begin{bmatrix} a_{11} & a_{12} \\ a_{21} & a_{22} \end{bmatrix}, \quad B = \begin{bmatrix} b_{11} & b_{12} \\ b_{21} & b_{22} \end{bmatrix} \tag{4.61c}$$

The elements of matrices A and B are given by

$$a_{11} = e^{-\beta\omega\Delta t_i} \left(\frac{\beta}{\sqrt{1-\beta^2}} \sin \omega\sqrt{1-\beta^2}\,\Delta t_i + \cos\omega\sqrt{1-\beta^2}\,\Delta t_i \right)$$

$$a_{12} = \frac{e^{-\beta\omega\Delta t_i}}{\omega\sqrt{1-\beta^2}} \sin\omega\sqrt{1-\beta^2}\,\Delta t_i$$

$$a_{21} = -\frac{\omega}{\omega\sqrt{1-\beta^2}} e^{-\beta\omega\Delta t_i} \sin\omega\sqrt{1-\beta^2}\,\Delta t_i \tag{4.61d}$$

$$a_{22} = e^{-\beta\omega\Delta t_i} \left(\cos\omega\sqrt{1-\beta^2}\,\Delta t_i - \frac{\beta}{\sqrt{1-\beta^2}} \sin\omega\sqrt{1-\beta^2}\,\Delta t_i \right)$$

$$b_{11} = e^{-\beta\omega\Delta t_i}\left[\frac{1}{\omega\sqrt{1-\beta^2}}\left(\frac{1}{\Delta t_i} - \beta\omega\right)\sin\omega\sqrt{1-\beta^2}\,\Delta t_i - \cos\omega\sqrt{1-\beta^2}\,\Delta t_i\right]$$

$$b_{12} = 1 - \frac{e^{-\beta\omega\Delta t_i}}{\omega\sqrt{1-\beta^2}\,\Delta t_i}\sin\omega\sqrt{1-\beta^2}\,\Delta t_i$$

$$b_{21} = e^{-\beta\omega\Delta t_i}\left[\frac{1}{\sqrt{1-\beta^2}}\left(\omega - \frac{\beta}{\Delta t_i}\right)\sin\omega\sqrt{1-\beta^2}\,\Delta t_i + \frac{1}{\Delta t_i}\cos\omega\sqrt{1-\beta^2}\Delta t_i\right] - \frac{1}{\Delta t_i} \qquad (4.61e)$$

$$b_{22} = e^{-\beta\omega\Delta t_i}\left[\frac{\beta}{\sqrt{1-\beta^2}\Delta t_i}\sin\omega\sqrt{1-\beta^2}\,\Delta t_i - \frac{1}{\Delta t_i}\cos\omega\sqrt{1-\beta^2}\,\Delta t_i\right] + \frac{1}{\Delta t_i}$$

From Eq. (4.56), the absolute acceleration, $\ddot{z}_i$, of the mass m at time t_i is given by

$$\ddot{z}_i = 2\beta\omega(\dot{y}_i - \dot{z}_i) + \omega^2(y_i - z_i) \qquad (4.62)$$

$(\dot{z}_i - \dot{y}_i)$ and $(z - y)$ in Eq. (4.62) respectively denote the relative velocity and relative displacement of the mass m. Hence, if the displacement and the velocity of the system are known at some time t_0, the state of the system at all subsequent times t_i can be computed exactly by a step-by-step application

of Eqs. (4.61) and (4.62). The computational advantage of this approach lies in the fact that the matrices A and B depend only on β, ω and Δt_i. If Δt_i, the interval of digitization, is constant (that is, the runway profile record is digitized at equal intervals), the computational efforts will still be simpler in the sense that the matrices A and B which consist of big expressions [Eqs. (4.61d) and (4.61e)] need to be evaluated only once at the beginning of the response calculation[8]. In the present investigation, the response is computed for the base displacement y_i measured at equal time intervals, Δt_i. The interval of integration, $\Delta\tau$, is chosen to be one-fifth of the interval of digitization Δt_i. The time interval of digitization is obtained as follows.

If the airplane, initially at rest, is moving at a constant acceleration 'a', then the total time taken to cover a distance's'is given by

$$t' = \sqrt{2s/a}$$

The time interval of digitization is given by

$$t = t'/N$$

where N is the total number of sample points.

4.3.2. Results

The response of the airplane moving with a constant acceleration 'a' during take-off is computed for a take-off distance of s = 300 ft. The runway profile is digitized at 2 ft. interval which gives N = 150. The response quantities computed are the maximum and the root-mean-square values of the relative displacement and the absolute acceleration of the mass m, which in a way respresent those at the cock-pit. The results are summarised as shown in Table 4.6.

CHAPTER 5

CONCLUSIONS

The thesis consists of two parts:

I. Measurement and calculations of power spectral density of runway roughness.

II. Response calculations of a light airplane to runway roughness during taxiing and take-off.

The measurement of runway roughness (I.I.T., Kanpur airstrip) has been carried out by two methods: (i) surveying and (ii) profilometer designed by Panchal[1]. The power spectral calculations of the roughness have been carried out on a digital computer. From the power spectral density curves (Fig. 2.5) it is observed that the roughness data obtained from surveying is good for longer wavelengths (4 ft. to 160 ft.) whereas the data from the profilometer measurement is good for smaller wavelengths (1.3 ft. to 16 ft.). The limitations on the range of wavelengths measurable by the profilometer are dictated by the characteristics of the pickup and the towing speed. It is found that at speeds greater than 25 m.p.h. the vehicle vibration becomes excessive. It is suggested that a multiwheel mounting[1] for the profilometer can be used to measure the roughness in longer wavelengths. The power spectral density curve obtained for the airstrip is found to agree well with the NATO curves.[15]

The response of a light aircraft (Piper) with a truss type of undercarriage during taxiing has been computed by the power spectral density method. The aircraft has been idealized to a five-degree-of-freedom lumped parameter system. The response parameters computed are the r.m.s. values of the absolute acceleration at the cockpit and the dynamic stresses in the undercarriage members. The primary contribution to the airplane response is found to be from the fundamental mode only. The response is found to increase as the taxiing speed is increased. The estimated maximum stresses in the members, with an exceedance probability of 0.27 percent, are found to be between 1.48 and 1.93 times the static stresses. The tyre stiffness is found to have a significant influence on the frequency and response calculations. The response increases as the tyre stiffness is increased. The fundamental frequency of the aircraft under study is found to lie between 2.112 and 2.983 cps for a tyre stiffness between 400 and 800 lbs./in. The absolute acceleration at the cockpit is found to lie between 0.150 g and 0.277 g for a tyre stiffness between 400 and 800 lbs./in. at a taxiing speed of 20 m.p.h.

For the response during take-off the airplane has been idealized to a single-degree-of-freedom spring-mass system. The excitation in this case is a non-stationary random process. The response (absolute acceleration at the cockpit)

is computed by numerically integrating the equation of motion. For a take-off speed of 40 m.p.h. and a take-off distance of 300 ft., the r.m.s. value and the maximum value of the absolute acceleration at the cockpit are found to be, respectively, 0.221 g and 0.369 g.

It can be concluded that the acceleration levels computed for the small aircraft during taxiing and take-off are within the tolerable limits. But, for larger flexible aircrafts the response will be critical to runway roughness during taxiing and take-off. The technique presented in this work can be used for determining the response of large aircrafts to runway roughness during taxiing and take-off. It will be interesting to calculate the response of aircrafts to runway roughness during landing also. The response during landing can be calculated by the same method used for calculating the response during take-off, i.e. by the numerical integration of the equation of motion. On the basis of the calculations of dynamic stresses presented in this thesis, the fatigue life of the undercarriage structure can be estimated.

REFERENCES

1. Panchal, H.K., 'Measurement and Power Spectral Analysis of Road Surface Profiles', M.Tech. Thesis, I.I.T., Kanpur, Aug. 1969.

2. Bendat, J.S., and Piersol, A.G., 'Measurement and Analysis of Random Data', John Wiley and Sons Pub., 1966.

3. Blackman, R.B. and Tukey, J.W., 'The Measurement of Power Spectra - From the Point of View of Communication Engineering', Dover Pub., 1958.

4. Thomson, W.E., 'Measurements and Power Spectra of Runway Roughness at Airports in Countries of the North Atlantic Treaty Organisation', NACA - TN 4303, July 1958.

5. Williams, D., 'An Introduction to the Theory of Aircraft Structures', Edward Arnold (Pub.) Ltd., London, 1960.

6. Hurty, W.C., and Rubinstein, M.F., 'Dynamics of Structures', Prentice Hall Pub., 1967.

7. Lin, Y.K., 'Probabilistic Theory of Structural Dynamics', McGraw-Hill Book Co., 1967.

8. Nigam, N.C., and Jennings, P.C., 'Digital Calculation of Response Spectra From Strong - Motion Earthquake Records', Technical Report, CALTECH, California, June 1968.

9. Tung, C.C., Penzien, J., Horonjeff, R., 'The Effect of Runway Uneveness on the Dynamic Response of

Supersonic Transports,' NASA CR-119, University of California, Berkeley, Oct. 1964.

10. Walls, J.H., Houbolt, J.C. and Press, H., 'Some Measurements and Power Spectra of Runway Roughness', NACA TN 3305, 1954.

11. Morris, G.J., and Stide, J.W., 'Response of a Light Airplane to Roughness of Unpaved Runways', NASA TN D-510, Sept. 1960.

12. Houbolt, J.C., Walls, J.H., and Smiley, R.F., 'On Spectral Analysis of Runway Roughness and Loads Developed During Taxiing', NASA TN 3484, 1955.

13. McKay, J.M., 'Measurements of Ground-Reaction Forces and Vertical Centre-of-gravity Accelerations of a Bomber Airplane Taxiing over Obstacles', NACA TN 4400, 1958.

14. Morris, G.J., 'Response of a Jet Trainer Aircraft to Roughness of Three Runways', NASA TN D-2203, 1964.

15. Taylor, J., 'Manual on Aircraft Loads', AGARD, North Atlantic Treaty Organization, Pergamon Press, 1965.

16. Kirk, C.L., and Perry, P.J., 'Analysis of Taxiing Induced Vibrations in Aircraft by the Power Spectral Density Method', The Aeronautical Journal, Royal Aero. Soc., March 1971.

TABLE 3.1: VALUES OF VARIOUS PARAMETERS USED IN THE PRESENT WORK.
THE VALUES ARE TYPICAL FOR A TWO-SEATER AIRCRAFT SUCH AS PIPER SUPER CUB. (REFER FIG. 3.2)

Member No.	1	2	3	4	5	6	7	8	9	10	11	12	
Length (in.)	116	125	34	27	15	34	34	15	27	34	125	116	
Area of cross section ($in.^2$)	-	1.0	.304	.338	.189	.189	.189	.189	.338	.304	1.0	-	
E ($lbs./in.^2$) x 10^6	11	11	30	30	30	30	30	30	30	30	11	11	
Mom. of inertia, I ($in.^4$)	60	-	-	-	-	-	-	-	-	-	-	60	

Wing stiffness, K_e (lbs./in.): 1319

Tyre stiffness, k (lbs./in.): 400, 600, 800

Masses (lbs.-$sec.^2$/in.): $m_1 = 0.4$, $m_2 = 0.052$, $m_3 = 3.63$, $m_4 = 0.052$, $m_5 = 0.4$

Critical damping factor, β: 0.025

Take-off speed = 40 m.p.h.; Take-off distance = 300 ft.; All up weight = 1750 lbs.

TABLE 4.1: NATURAL FREQUENCIES AND MODE SHAPES OF THE IDEALIZED MODEL (FIG. 3.2).
(CASE: TYRE STIFFNESS k = 400 lbs./in.)

No.		1	2	3	4	5
Natural Frequency (cps)		2.112	30.068	33.151	350.819	355.445
Mode Shape	z_1	0.47183	1.11803	1.01360	0	-0.00063
	z_2	0.46877	0	-0.22012	-3.10805	-3.06461
	z_3	0.46950	0	-0.21850	0	0.08751
	z_4	0.46877	0	-0.22012	3.10805	-3.06461
	z_5	0.47183	-1.11803	1.01360	0	-0.00063

TABLE 4.2 : STANDARD DEVIATION OF ABSOLUTE ACCELERATION AT THE COCKPIT AND DYNAMIC STRESSES IN THE UNDERCARRIAGE MEMBERS AT VARIOUS CONSTANT TAXIING SPEEDS

(CASE: TYRE STIFFNESS k = 400 lbs./in.)

Taxiing speed (m.p.h.)	Abs. Accln. at cockpit (g=386 in./sec.^{2})	Dynamic stress, σ_D (lbs./in.^{2}) Member: 2	3	4	5	6	7	8	9	10	11
10	0.119 g	43.64	189.70	300.40	49.84	80.35	80.35	49.84	300.40	189.70	43.64
20	0.150 g	55.37	240.45	380.12	68.48	101.4	101.4	68.48	380.12	240.45	55.37
30	0.200 g	74.16	318.94	505.98	82.50	133.7	133.7	82.50	505.98	318.94	74.16
Static stress, (μ_S) (Mean stress) (lbs./in.^{2})		-236.50	-1490.0	-2363	-221.5	-628	-628	-221.5	-2363	-1490	-236.5

TABLE 4.3. : PROBABILITY OF EXCEEDANCE OF DYNAMIC STRESS

Stress	σ_D	$2\sigma_D$	$3\sigma_D$
Prob. of Exceedance	31.73 %	4.55 %	0.27 %

TABLE 4.4: RATIOS OF ESTIMATED MAXIMUM DYNAMIC STRESS* TO STATIC STRESS (CASE: TYRE STIFFNESS, k = 400lbs./in.)

Member No.		2	3	4	5	6	7	8	9	10	11
Ratio: $\frac{\mu_S + 3\sigma_D}{\mu_S}$	10 m.p.h.	1.55	1.38	1.38	1.68	1.38	1.38	1.68	1.38	1.38	1.55
	20 m.p.h.	1.70	1.48	1.48	1.93	1.48	1.48	1.93	1.48	1.48	1.70

* Estimated Max. Dyn. Stress = $|\mu_S| + 3\sigma_D$

TABLE : 4.5. – EFFECT OF TYRE STIFFNESS ON FUNDAMENTAL FREQUENCY AND ABSOLUTE ACCELERATION AT THE COCKPIT (CASE: TAXING SPEED = 20 m.p.h.)

Tyre stiffness lbs./in.	Fundamental Frequency (cps)	Abs. Accln. at cockpit
400	2.112	0.150 g
600	2.585	0.213 g
800	2.983	0.277 g

TABLE 4.6 : RESPONSE DURING TAKE-OFF

1. Relative Displacement of mass m:
   (i) r.m.s. value = 0.3425 in.
   (ii) max. value = 0.8228 in.
2. Absolute Acceleration of mass m:
   (i) r.m.s. value = 0.221 g
   (ii) max. value = 0.369 g.

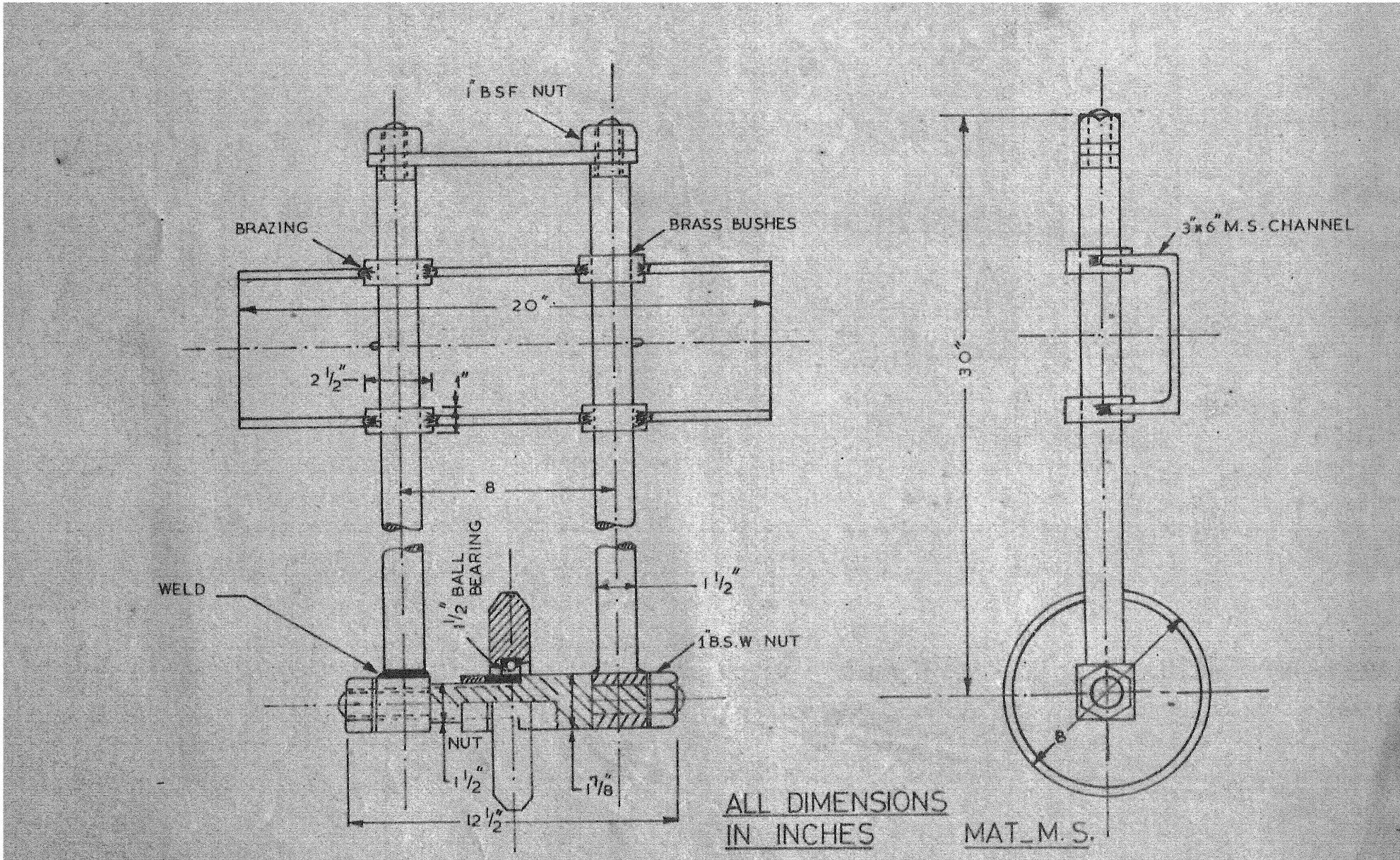

FIG. 2.1_FIGURE SHOWS THE ASSEMBLY OF THE PROFILE FOLLOWER (REF.1)

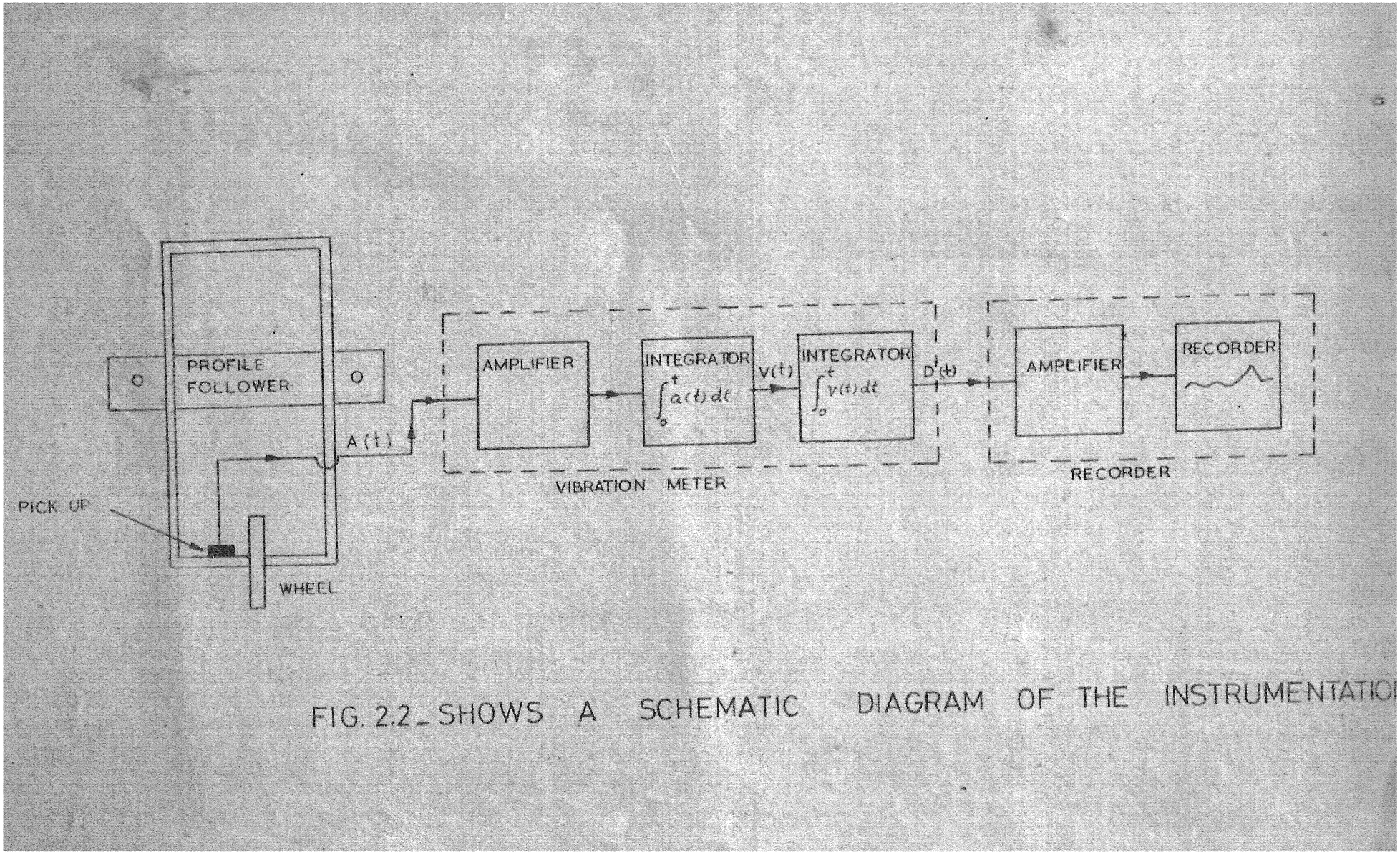

FIG. 2.2 - SHOWS A SCHEMATIC DIAGRAM OF THE INSTRUMENTATIO

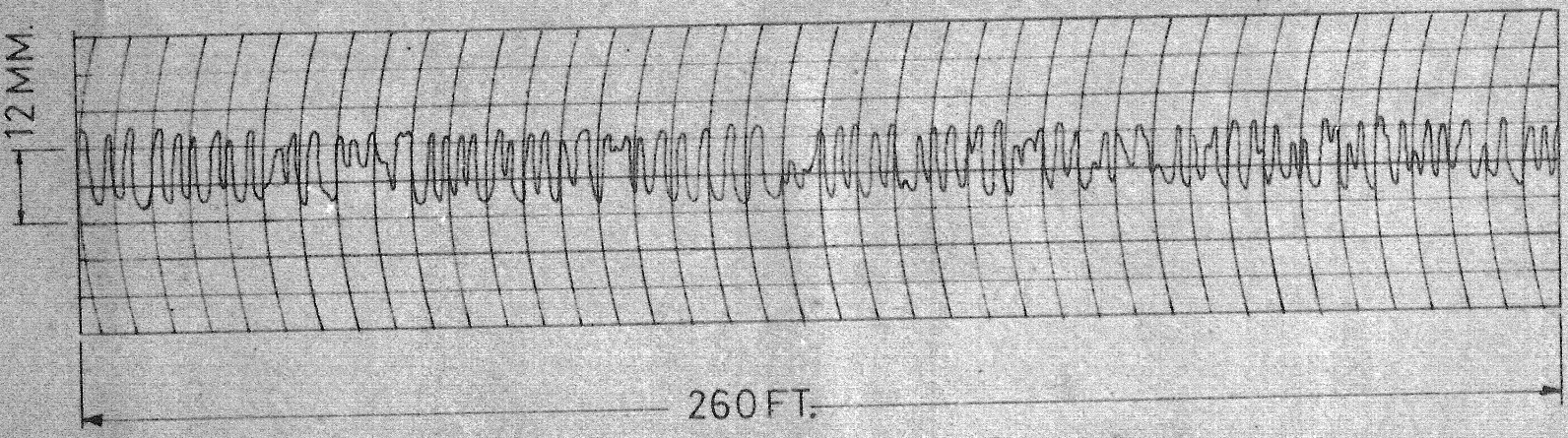

FIG. 2.3 — A SAMPLE OF RUNWAY PROFILE RECORD OBTAINED FROM PROFILOMETER MEASUREMENTS

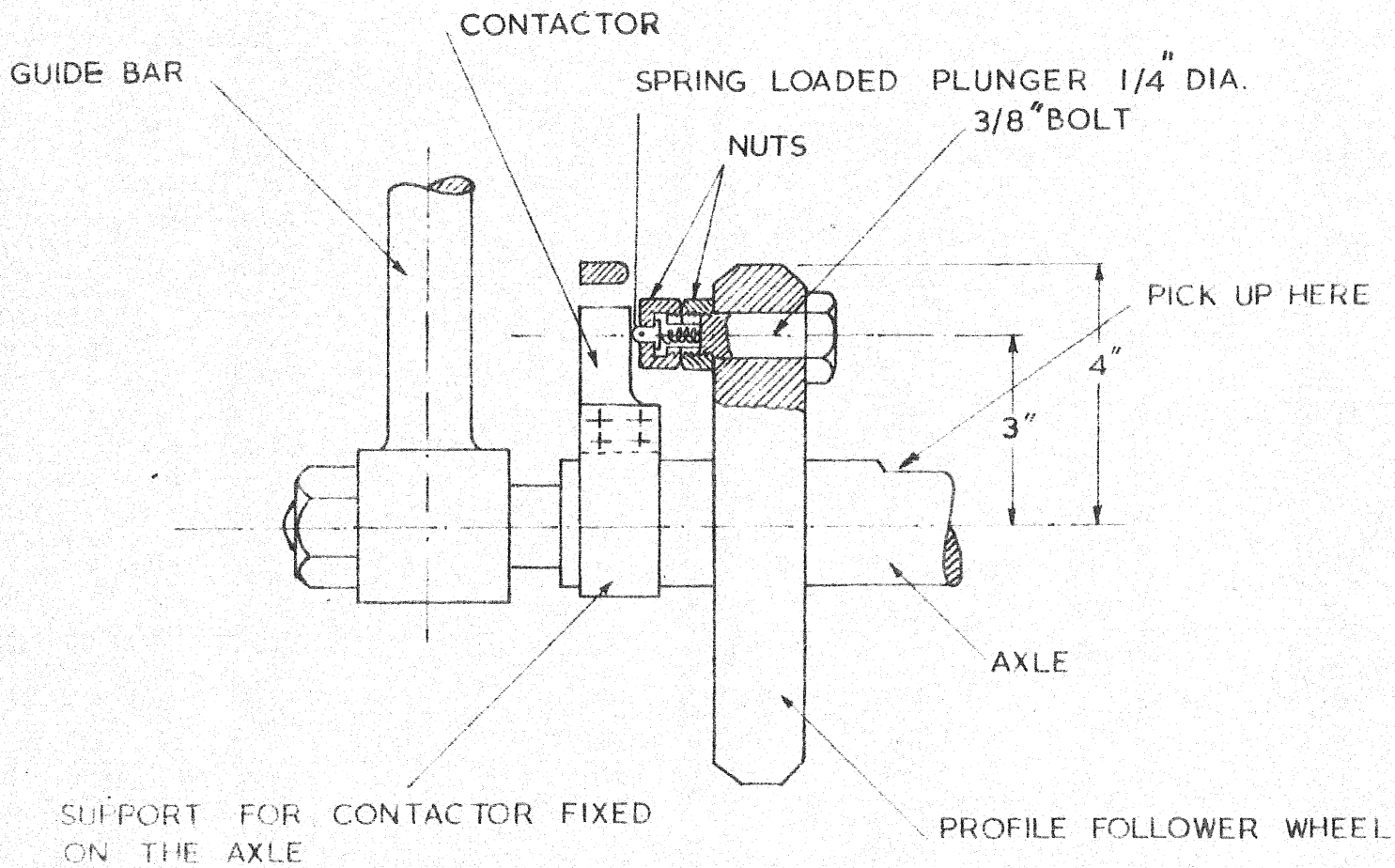

FIG. 2.4 'MAKE AND BREAK' CONTACTOR OR 'TIMER' ATTACHED TO PROFILE FOLLOWER.

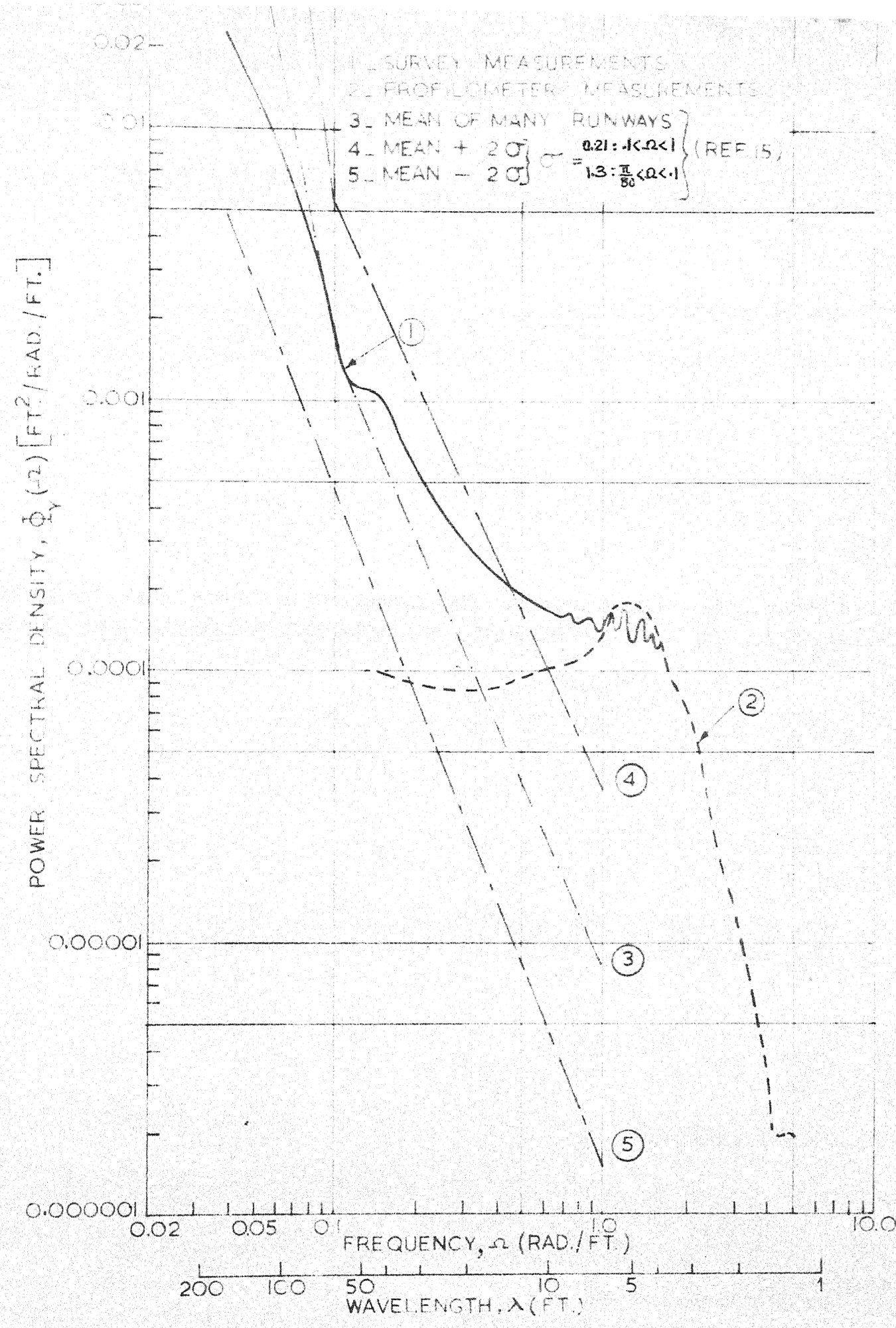

FIG. 2.5_ POWER SPECTRAL DENSITY OF RUNWAY ROUGHNESS.

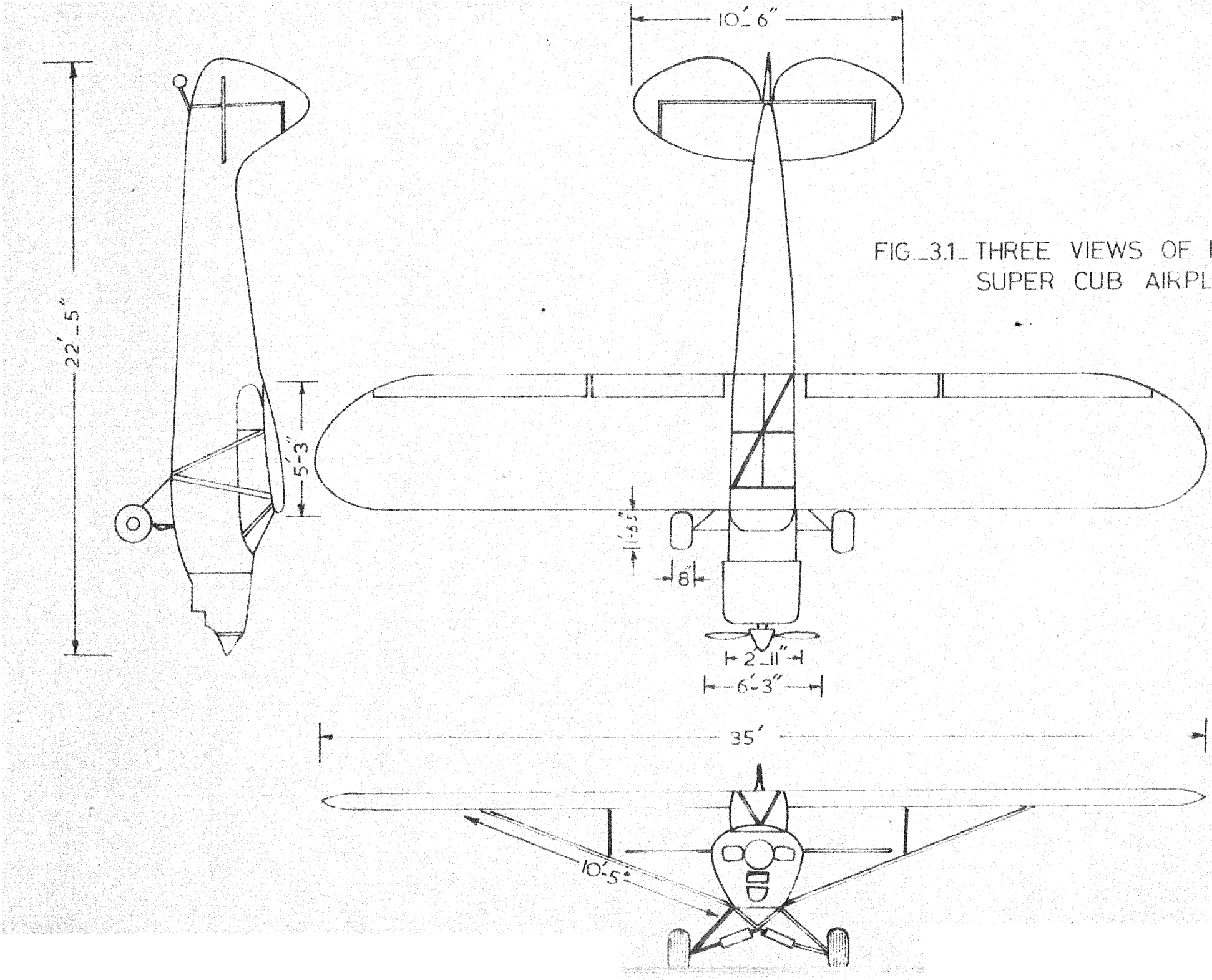

FIG. 3.1 THREE VIEWS OF PIPER SUPER CUB AIRPLANE

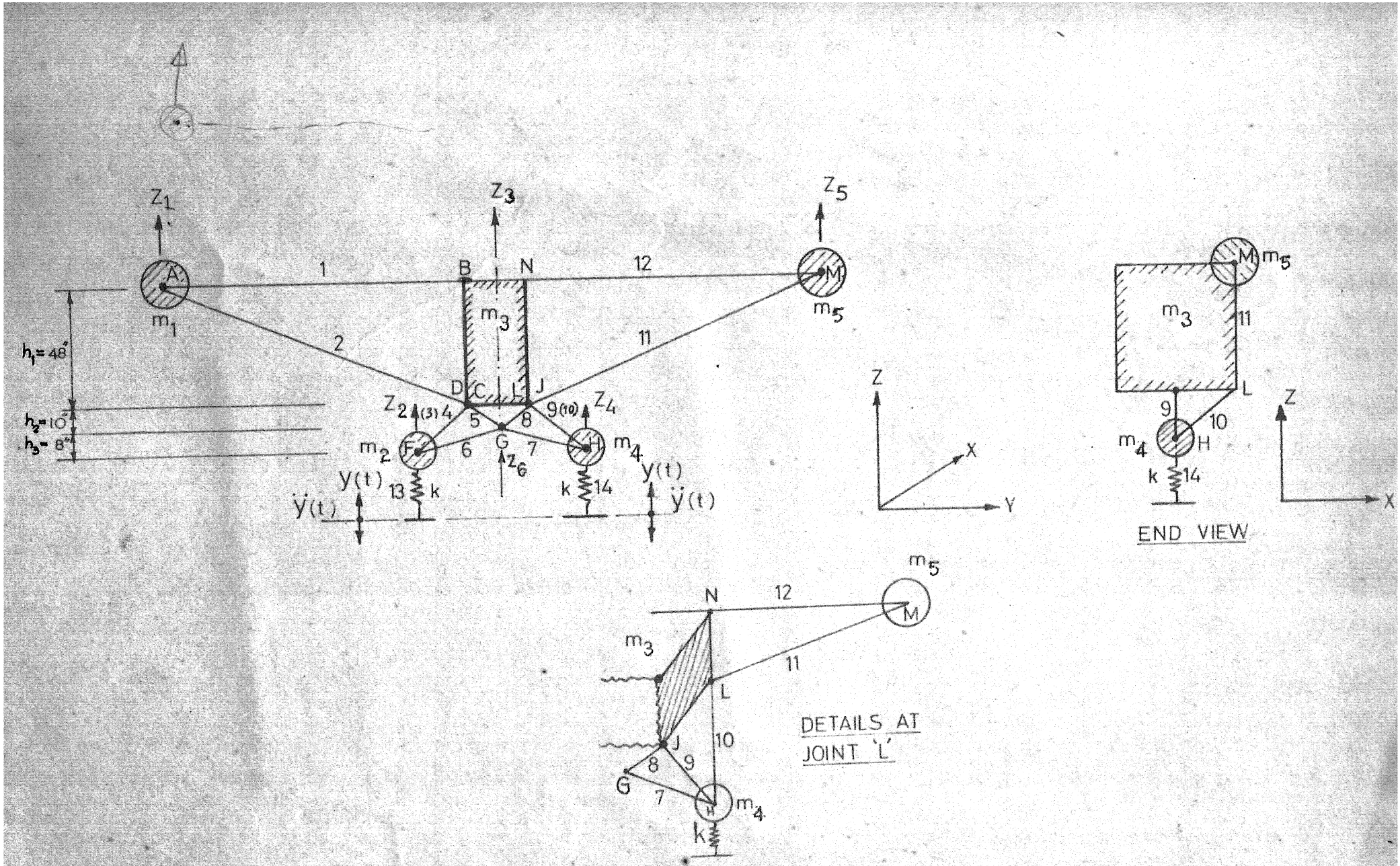

FIG. 3.2 IDEALIZED MODEL OF PIPER AIRPLANE

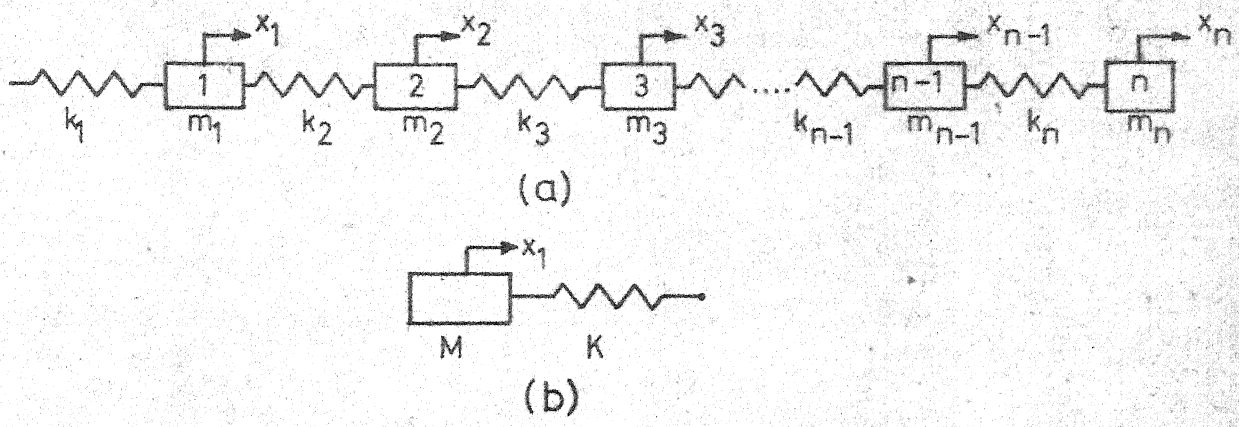

FIG. 3.3 (a) SPRING - MASS SYSTEM (n d.o.f.)
(b) EQUIVALENT SYSTEM (1 d.o.f.)

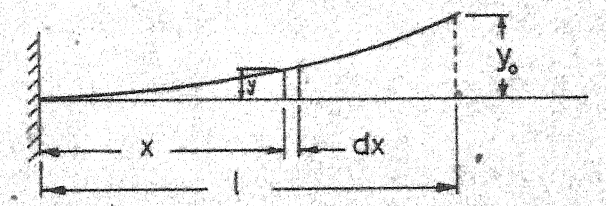

FIG. 3.4 _ CANTILEVER

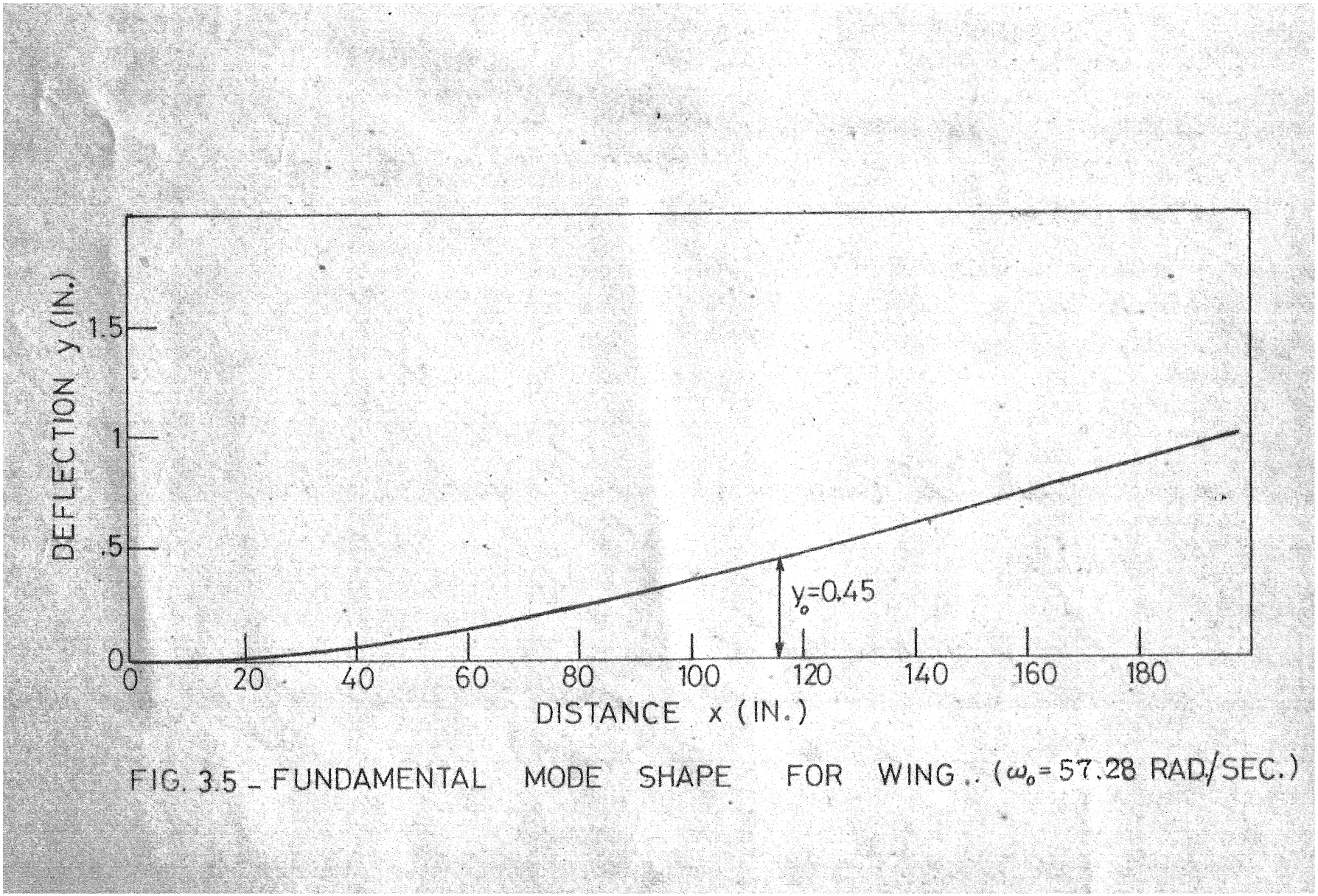

FIG. 3.5 – FUNDAMENTAL MODE SHAPE FOR WING .. (ω_o = 57.28 RAD/SEC.)

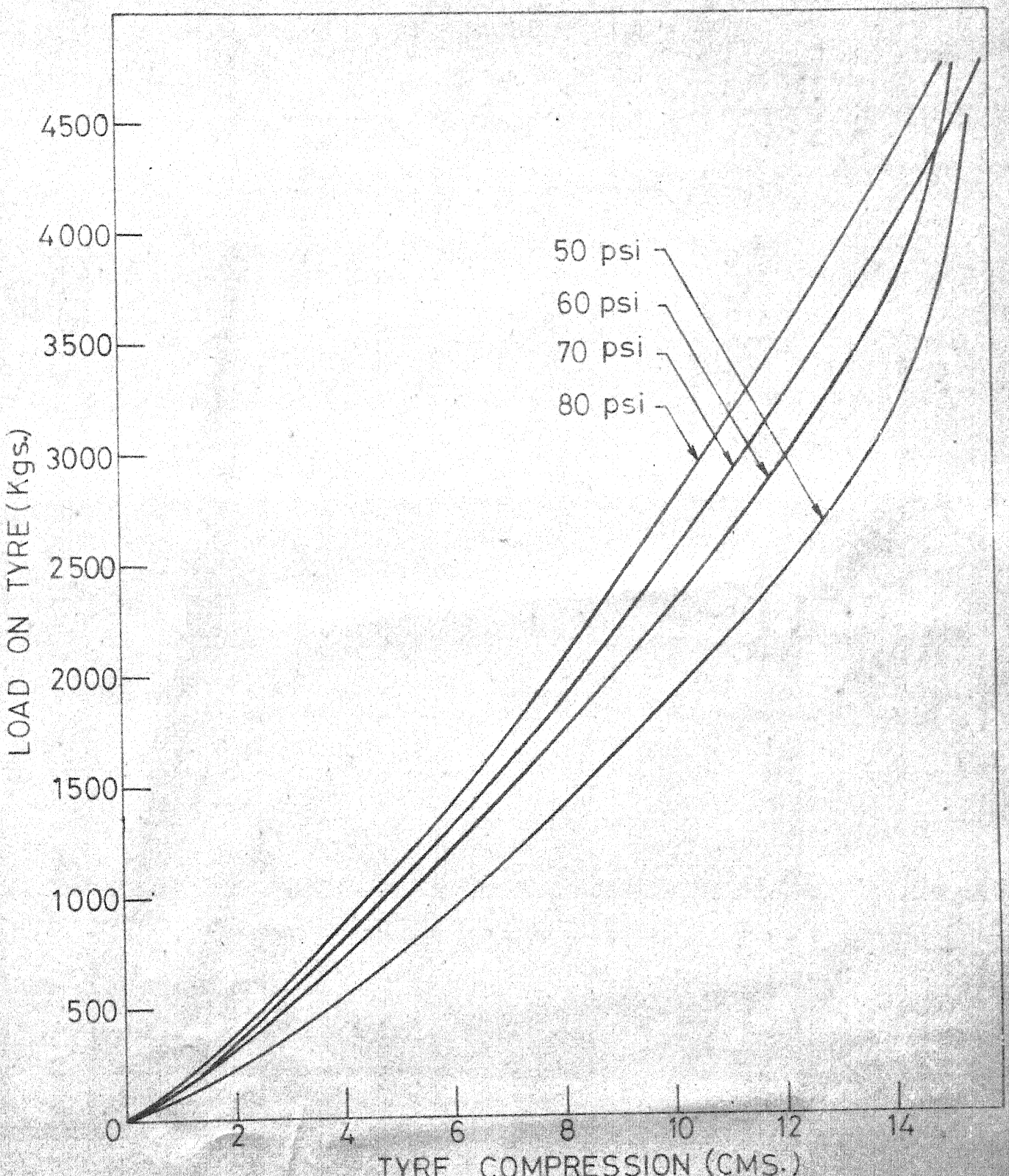

FIG. 3.6 _ LOAD DISPLACEMENT CURVES FOR AN AIRPLANE TYRE AT VARIOUS TYRE PRESSURES.
TYRE: DUNLOP _ 26 x 7.75 _ 13 _ 8 PLY RATING.

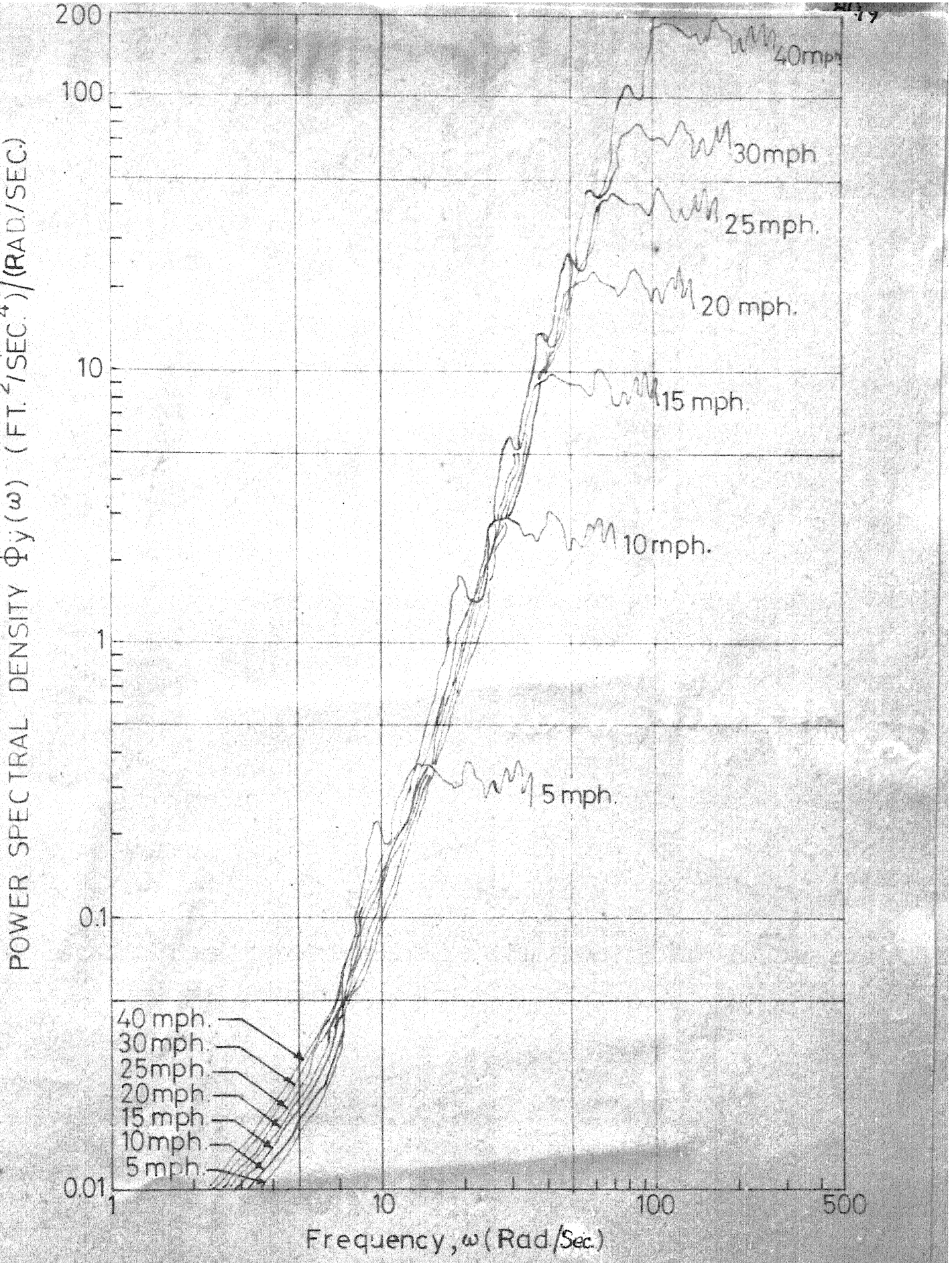

FIG._4.1_POWER SPECTRAL DENSITY OF BASE ACCELERATION AT DIFFERENT TAXYING SPEEDS

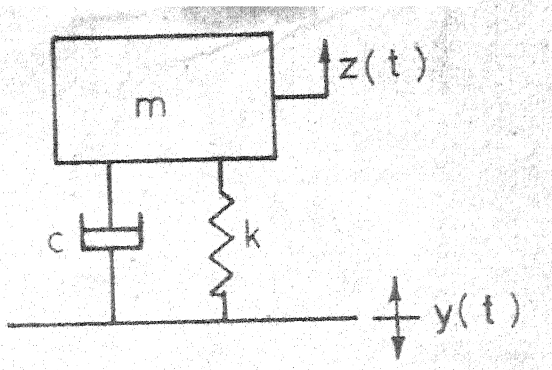

FIG. 4.2 _ SINGLE - DEGREE - OF - FREEDOM SYSTEM.

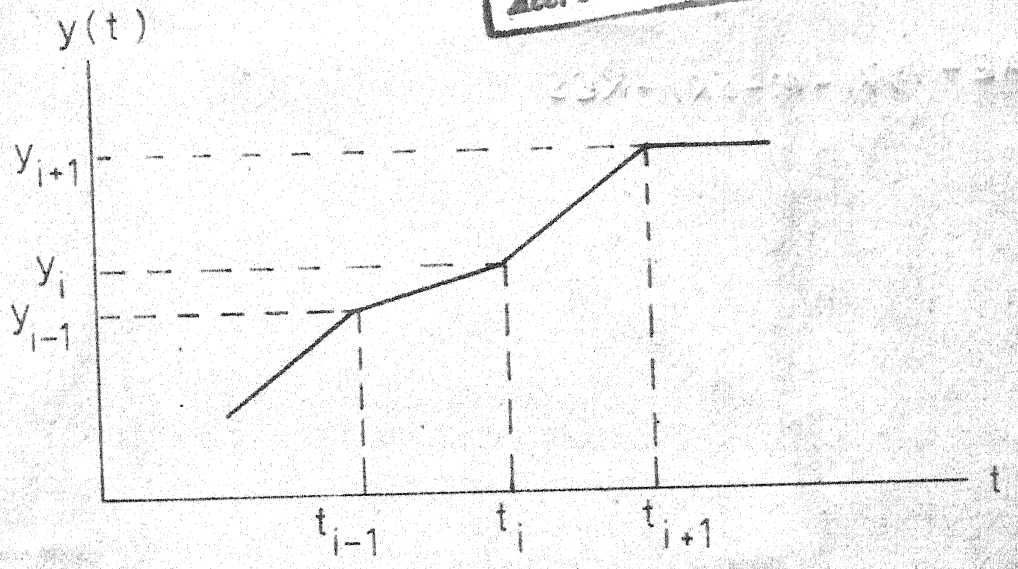

FIG. 4.3 _ IDEALIZED BASE DISPLACEMENT